JOURNAL OF GEOPHYSICAL RESEARCH, VOL. 107, NO. D20, 4442, doi:10.1029/2001JD001471, 2002

A climatology of stratospheric polar vortices and anticyclones

V. Lynn Harvey
Science Applications International Corporation, Hampton, Virginia, USA

R. Bradley Pierce and T. Duncan Fairlie
NASA Langley Research Center, Hampton, Virginia, USA

Matthew H. Hitchman
Department of Atmospheric and Oceanic Sciences, University of Wisconsin - Madison, Madison, Wisconsin, USA

Received 7 November 2001; revised 11 February 2002; accepted 12 February 2002; published 29 October 2002.

[1] United Kingdom Meteorological Office global analyses from 1991 to 2001 are used to create a global climatology of stratospheric polar vortices and anticyclones. New methodologies are developed that identify vortices in terms of evolving three-dimensional (3-D) air masses. A case study illustrates the performance of the identification schemes during February and March of 1999 when a merger of anticyclones led to a stratospheric warming that split the Arctic polar vortex. The 3-D structure and temporal evolution of the Arctic vortex and identified anticyclones demonstrates the algorithm's ability to capture complicated phenomena. The mean geographical distribution of polar vortex and anticyclone frequency is shown for each season. The frequency distributions illustrate the climatological location and persistence of polar vortices and anticyclones. A counterpart to the Aleutian High is documented in the Southern Hemisphere: the "Australian High." The temporal evolution of the area occupied by polar vortices and anticyclones in each hemisphere is shown as a function of potential temperature. Large polar vortex area leads to an increase in anticyclone area, which in turn results in a decrease in the size of the polar vortex. During Northern winter and Southern spring, 9 years of daily anticyclone movement are shown on the 1200 K (36 km, 4 hPa) isentropic surface. Preferred locations of anticyclogenesis are related to cross-equatorial flow and weak inertial stability. Regimes of traveling and stationary anticyclones are discussed. *INDEX TERMS:* 3309 Meteorology and Atmospheric Dynamics: Climatology (1620); 3319 Meteorology and Atmospheric Dynamics: General circulation; 3334 Meteorology and Atmospheric Dynamics: Middle atmosphere dynamics (0341, 0342); *KEYWORDS:* polar vortex, stratospheric anticyclones

Citation: Harvey, V. L., R. B. Pierce, and M. H. Hitchman, A climatology of stratospheric polar vortices and anticyclones, *J. Geophys. Res.*, *107*(D20), 4442, doi:10.1029/2001JD001471, 2002.

1. Introduction

[2] Strong coherent vortices trap fluid in their cores and isolate it for long times while they transport it unmixed over great distances [*Weiss*, 1991a; *Elhmaidi et al.*, 1993; *Provenzale*, 1999, and references therein]. Examples include Gulf Stream rings in the ocean [*Dewar and Flierl*, 1985], vortex rings generated in a water tank [*Domon et al.*, 2000], baroclinic waves in the troposphere [*Thorncroft et al.*, 1993; *Wang and Shallcross*, 2000], stratospheric polar vortices [*Hartmann et al.*, 1989; *Schoeberl et al.*, 1992; *Paparella et al.*, 1997], and long-lived stratospheric anticyclones [*Hsu*, 1980; *Manney et al.*, 1995a; *Morris et al.*, 1998]. While there is rapid mixing at the edge, robust and persistent anticyclones have been observed to isolate air for weeks at a time in their cores [*Manney et al.*, 1995a; *Morris et al.*, 1998] permitting chemical conditions within them that are significantly different from the surrounding ambient air.

[3] Large quasi-stationary anticyclones are a common feature of the winter stratospheric circulation [e.g., *Labitzke*, 1981a; *Pawson et al.*, 1993; *Harvey and Hitchman*, 1996] and their structure and behavior have been extensively documented on a case-by-case basis [e.g., *Boville*, 1960; *Hirota et al.*, 1973; *Labitzke*, 1981b; *O'Neill and Pope*, 1988]. These anticyclonic vortices are known to wrap together filaments of tropical air and polar vortex air [*Pierce and Fairlie*, 1993; *Lahoz et al.*, 1996; *Waugh et al.*, 1994; *Polvani et al.*, 1995; *Manney et al.*, 1995a, 1995b, 2000] and homogenize tracer gradients within them [*Lahoz et al.*, 1996]. The mixing efficiency on the edge of stratospheric anticyclones and the interaction between anticyclones and the polar vortices has important implications for the general stratospheric circulation, the lifetime of the ozone hole, the extent of midlatitude ozone loss [*Degorska and Rajewska-Wiech*, 1996], and the mixing timescales of aircraft effluent.

0148-0227/02/2001JD001471$09.00

[4] Stratospheric anticyclones are present and interact with the polar vortex in a variety of situations. Stratospheric "surf zones," for example, [*McIntyre and Palmer*, 1984] are generally not zonally symmetric in midlatitudes but result from the presence of one or more large-scale, quasi-stationary anticyclones [*Fairlie and O'Neill*, 1988]. Thus, in the discussion of planetary wave breaking (PWB) [*McIntyre and Palmer*, 1983], the presence and involvement of anticyclones needs to be emphasized [see also *O'Neill and Pope*, 1988; *O'Neill et al.*, 1994]. This PWB process is efficient at irreversibly mixing air of different origins, however, the strongest mixing does not necessarily occur in the core of anticyclones. Regions of "chaotic advection" [*Pierce and Fairlie*, 1993] occur along the periphery of anticyclones. Stratospheric anticyclones also play a critical role in the following processes. They create high latitude nonlinear critical layers [*Salby et al.*, 1990] along their central latitude. The "Kelvins cats eye" solution [*Warn and Warn*, 1978] is a closed anticyclonic circulation [*O'Neill and Pope*, 1988]. Cross-equatorial flow, visible in tracer fields [*Randel et al.*, 1993; *Chen et al.*, 1994], and the movement of material lines [*Waugh*, 1993], are associated with anticyclonic air with low isentropic potential vorticity (PV). Zonal harmonic waves 1 and 2 otherwise refer to 1 or 2 anticyclones present around a latitude circle. Anticyclones have long been regarded as important in the development of sudden stratospheric warmings (SSW) [e.g., *Scherhag*, 1952; *Labitzke*, 1977, 1981a, 1981b; *McIntyre*, 1982], a phenomenon characterized by rapid warming and deceleration of the polar night jet (PNJ). In particular, "Canadian" type warmings are due to the intensification of the Aleutian High (hereafter AH) [*Labitzke*, 1977].

[5] Climatological studies of tropospheric cyclones and anticyclones include those of *Bell and Bosart* [1989], *Murray and Simmonds* [1991], *Price and Vaughan* [1992], *Jones and Simmonds* [1993, 1994], and *Sinclair* [1994, 1995, 1996, 1997]. In studies such as these, an objective way to determine the areal extent of a vortex is required and resulting frequency distributions are directly related to the identification criteria used. Such methods include the use of pressure extrema or pressure gradients [*Lambert*, 1988; *Sinclair*, 1994, 1996; *Murray and Simmonds*, 1991], closed geopotential height contours [*Bell and Bosart*, 1989; *Price and Vaughan*, 1992], and vorticity thresholds [*Jones and Simmonds*, 1994; *Sinclair*, 1995, 1997]. While much attention has been given to locate the edge of stratospheric polar vortices [*Manney and Zurek*, 1993; *Manney et al.*, 1994; *Norton and Carver*, 1994; *Rummukainen et al.*, 1994; *Dameris and Grewe*, 1994; *Dameris et al.*, 1995; *Yang*, 1995; *Trounday et al.*, 1995; *Nash et al.*, 1996; *Paparella et al.*, 1997; *Waugh*, 1997; *Michelsen et al.*, 1998, 1999; *Waugh and Randel*, 1999; *Waugh et al.*, 1999; *Polvani and Saravanan*, 2000; *Koh and Plumb*, 2000], the same sort of attention has not been paid to stratospheric anticyclones. The climatology presented here builds on past ones such as that of *Waugh and Randel* [1999] in that it documents the climatological distribution of stratospheric anticyclones in addition to the polar vortices.

[6] The format of the paper is as follows. Section 2 describes the United Kingdom Meteorological Office (UKMO) data and the algorithms developed to identify polar vortices and anticyclones. A case study is shown in section 3 to illustrate the performance of the algorithms and show the structure of the Arctic vortex and anticyclones during a dynamically active time. A 10-year climatology of polar vortex and anticyclone frequency is then presented in section 4. The climatological evolution of polar vortex and anticyclone area is shown in section 5 as a function of potential temperature. The remainder of the paper focuses on the anticyclone statistics. Section 6 describes the daily motion of anticyclone centers for 9 Northern hemisphere (NH) winter and Southern hemisphere (SH) spring seasons on the 1200 K isentropic surface, a representative altitude halfway between the tropopause and the stratopause. In section 7 stationary and traveling components of identified anticyclones are discussed. Section 8 summarizes the results of the study and mentions possible avenues of future research.

2. Data

2.1. UKMO Correlative Analyses

[7] UKMO correlative analyses of temperature, geopotential height, and wind developed for the Upper Atmosphere Research Satellite (UARS) project are used in this study. These data are currently available from 17 October 1991 to 30 September 2001 and are valid once daily at 12 GMT. The spatial resolution is 2.5° latitude by 3.75° longitude on the following 22 pressure levels: 1000 to 0.316 hPa in increments of $1000 \times 10^{-i/6}$, where i = 0 to 21. The vertical resolution is 2.5 km. Details of this data set are given by *Swinbank and O'Neill* [1994]. Geopotential height, temperature, and winds are linearly interpolated from isobaric surfaces to the following potential temperature surfaces: 330–400 K by 10 K, 400–550 K by 25 K, 600 to 1000 by 100 K, and 1000 to 2000 by 200 K. The velocity field is decomposed into rotational and divergent components from which the scalar stream function (ψ) field is used to characterize the large scale flow. Isopleths of ψ are parallel to the rotational component of the wind. In addition, PV and the Q diagnostic (described in the next subsection) are calculated. From 330–550 K (9–22 km, 310–40 hPa) the vertical resolution is ≈1 km. From 550–2000 K (22–50 km, 40–0.75 hPa) there are 2–3 km between theta surfaces.

2.2. The Q Diagnostic

[8] The scalar quantity Q is a measure of the relative contribution of strain and rotation in the wind field [*Fairlie*, 1995; *Fairlie et al.*, 1999]. Q is derived by separating the velocity gradient tensor, $\mathbf{L}$, into the rate of deformation tensor, $\mathbf{D} = 1/2\ (\mathbf{L} + \mathbf{L}^t)$, and the solid body spin tensor, $\mathbf{W} = 1/2\ (\mathbf{L} - \mathbf{L}^t)$ [see *Malvern*, 1969]. In tensor notation, $2Q = \mathbf{D} : \mathbf{D} - \mathbf{W} : \mathbf{W}$ where the operator ":" represents the tensor scalar product. Neglecting the vertical component, Q is given by,

$$Q = \frac{1}{2}\left(\frac{1}{a\cos\phi}\frac{du}{d\lambda} - \frac{v}{a}\tan\phi\right)^2 + \frac{1}{2}\left(\frac{1}{a}\frac{dv}{d\phi}\right)^2 + \left(\frac{1}{a^2\cos\phi}\frac{du}{d\phi}\frac{dv}{d\lambda} + \frac{u\tan\phi}{a^2}\frac{du}{d\phi}\right)$$

where ϕ = latitude; λ = longitude, u = zonal wind, v = meridional wind, and a = the radius of the Earth. Q is

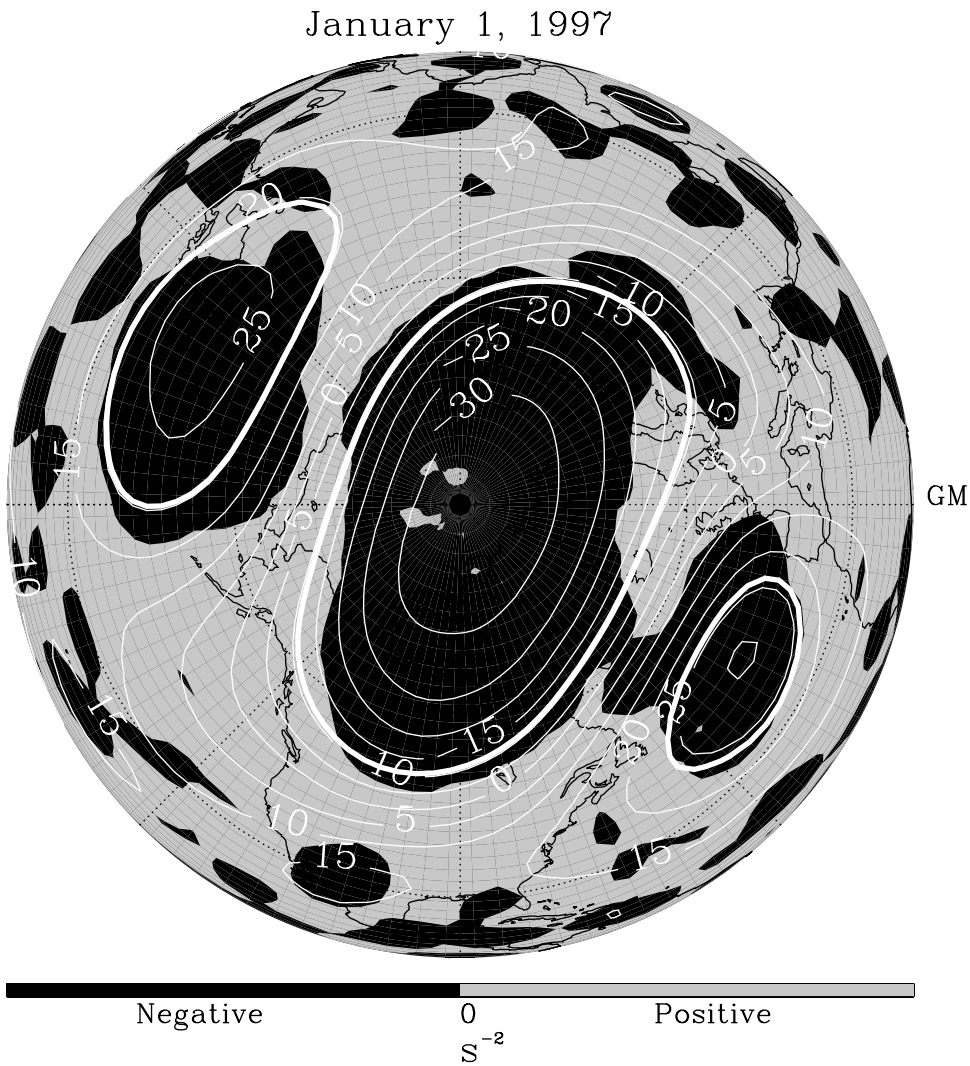

Figure 1. Northern Hemisphere Q (shaded) and stream function (contoured) on the 1000 K isentropic surface. Thick contours represent the edges of the Arctic vortex and anticyclones. Stream function contours are in intervals of 5×10^7 m^2 s^{-1}.

positive (negative) where strain (rotation) dominates the flow. For example, shear zones on the edges of vortices and near jet streams have positive Q while negative Q is associated with stable rotational flow [*Weiss*, 1991b; *Babiano et al.*, 1994]. Q has been used to study coherent vortices in two dimensional turbulence [*McWilliams*, 1984; *Brachet et al.*, 1988; *Elhmaidi et al.*, 1993] and stratospheric dynamics [*Haynes*, 1990; *Fairlie*, 1995; *Paparella et al.*, 1997; *Fairlie et al.*, 1999]. Figure 1 is an orthographic projection of the NH and shows Q (shaded) and ψ (contours) fields with vortex edges superimposed on 1 January 1997 at 1000 K, which is near 32 km or 5 hPa. This example of ψ and Q represents a typical NH winter day. Negative Q is found in the interior of the Arctic vortex and anticyclones while the PNJ is associated with positive Q. While Q is generally negative inside vortices, there are often interior shear zones observed. These zones are particularly common in the presence of elongated polar vortices and polar vortex division, elongated anticyclones, and anticyclone merger events. For this reason it is necessary to integrate Q around ψ isopleths to define vortices instead of simply using regions of negative Q. Here, $\{\oint Q = 0\}$ delineates vortex edges.

2.3. Vortex Identification Algorithms

2.3.1. Polar Vortices

[9] Q is more effective at identifying vortex edges when the circulation is strong and shear zones are well defined. This is often the case in the middle and upper stratosphere and when the vortex is cold. In the lower stratosphere and during vortex formation and decay, the Q field is more complex and integration around ψ isopleths is a poor indicator of the circulation. It is therefore useful to also integrate wind speed along ψ isopleths and use this quantity in conjunction with $\oint Q$ to identify the polar vortices. Relative vorticity (ζ) is also integrated along ψ isopleths to ensure that the circulation is cyclonic. An equatorward boundary at 15° is imposed and ψ isopleths that intersect this boundary are not considered. ψ contours where $\oint Q$ changes sign are vortex edge candidates. There are typically 2–4 candidate isopleths on each level per day. Of the candidate isopleths having cyclonic $\oint \zeta$, the one with

the largest integrated wind speed is considered the vortex edge. Below 450 K (17 km or 100 hPa) the presence of the subtropical jet contaminates edge identification.

[10] The algorithm is also tested using isopleths of PV instead of ψ isopleths. The two algorithms are generally consistent on a day to day basis, however, differences occur during dynamically active times. Seasonal zonal mean differences in the resulting frequency distributions are less than 20%. Differences may be due to the PNJ being more colocated with ψ than with PV contours. An advantage of using ψ isopleths is that ψ contours tend to be smooth. PV is a more complicated field and using PV isopleths results in a vortex with holes, jagged edges, and detached material in midlatitudes. An advantage of using PV contours is that PWB is captured more often. The climatology presented here is the result of integrating around ψ isopleths.

2.3.2. Anticyclones

[11] Unlike polar vortices, it is common for multiple anticyclones to be present on a given day and altitude. Matters are complicated when there are more than one closed ψ isopleth with the same value encircling different anticyclones. In this situation, the physical interpretation of $\oint Q < 0$ is less clear. One cannot be sure that the isopleth would have $\oint Q < 0$ if each anticyclone is considered separately. Therefore, $\oint Q$ needs to be evaluated one anticyclone at a time. To accomplish this we adopt the following algorithm. Instead of considering a hemispheric domain, each hemisphere is sectioned off into 90° longitude sectors that sweep eastward in 30° increments through as many as 4 complete revolutions around the hemisphere. When an anticyclone is identified in a sector the sector sweeps a distance such that the western edge of the next sector is adjacent to the eastern edge of the current sector. This is done to avoid searching in a sector that contains a portion of a previously identified anticyclone.

[12] The following steps are performed in each sector. $\oint Q$ and $\oint \zeta$ are calculated for each ψ isopleth. The algorithm is not sensitive to the ψ contour interval. Using half as many isopleths resulted in less than a 2% difference in anticyclone frequency. If there is more than one ψ isopleth with the same value in a sector the domain is reduced to include only the poleward-most contour. If an isopleth intersects a sector boundary then that boundary expands in 10° increments until the contour is fully resolved. The isopleth is excluded if, during expansion, (1) a sector boundary comes in contact with a previously identified anticyclone before the current ψ contour is enclosed by the sector, or if (2) sector width exceeds 180°. This zonal limit acts to exclude weak zonally broad cross-equatorial circulations, however, it is also a limitation of the algorithm in that circumpolar anticyclones are not identified. This situation will be allowed in subsequent versions of the algorithm. Circumpolar anticyclones are observed during SSW events and in the summer. ψ isopleths are also excluded if, (3) $\oint Q > 0$, (4) $\int Q dA > 0$, (5) $\oint \zeta$ is cyclonic, or (6) the area enclosed spans less than 15° longitude or 10° latitude. From the family of isopleths that are not excluded, the outermost ψ contour defines the edge of the anticyclone.

[13] The algorithms generate a gridded field where grid points inside polar vortices are given a value of 1, grid points inside anticyclones are given values of -1, -2, -3,... where each integer earmarks a different anticyclone. If there is only one anticyclone present there are only -1 values. Grid points outside vortices are set to 0. We refer to this field as the "vortex marker" field. Climatological frequency is presented as a percent of time that the polar vortex or an anticyclone exists at a given grid point. Frequency and area statistics result from this analysis, however, the strength of polar vortices and anticyclones is not considered here. This is left as a topic of future study. Frequency and area diagnostics provide the opportunity to quantify interannual variability and to calculate trends in the number and size of polar vortices and anticyclones. Stratospheric ozone loss acts to cool the stratosphere and, in turn, increase the lifetime of stratospheric polar vortices [*Randel and Wu*, 1999; *Zhou et al.*, 2000]. In the troposphere, a decrease in Antarctic sea-ice concentration has been shown to effect the frequency and strength of tropospheric cyclones [e.g., *Simmonds and Wu*, 1993]. Thus, trend analyses of a long, continuous record of the "vortex marker" field will likely provide inferences into such global climate changes.

[14] Figure 2 shows Arctic vortex and AH edges contoured on 9 overlapping potential temperature surfaces, from ≈20 to ≈50 km, on 12 January 2000. The three-dimensional (3-D) structure of the Arctic vortex/AH system on this day is a representative example of NH winter days in the stratosphere. Material lines are initialized 5 days earlier inside the AH and passively advected to their current locations. The dynamical edge definition agrees well with the location of the kinematic edge as determined from these trajectory calculations. While the algorithm successfully captures the circulations themselves it is important to realize that the vortex edges are fundamentally permeable.

3. Case Study During February and March 1999

[15] This section assesses the performance of the vortex identifier algorithms for the specific case of February and March 1999 in the Arctic. The Arctic vortex and anticyclones are depicted as "objects" evolving in 3-D and represent discrete closed circulations.

[16] During this case study two anticyclones merge and the Arctic vortex subsequently splits in two. This 1999 case demonstrates the ability of the algorithms to identify vortices despite a high degree of dynamical activity. It will be shown that the Arctic vortex and anticyclones are successfully identified during an anticyclone merger, the division of the Arctic vortex, and extreme transience. Other such time periods are similarly captured. Note, the algorithms perform even more consistently during quiescent times. The synoptic evolution during December 1998 and January 1999, preceding the time period shown here is given by [*Manney et al.*, 1999]. They provide a detailed discussion of the December 1998 SSW that also divided the vortex and its recovery in January. They also note that the 1998/1999 Arctic vortex was the warmest and weakest in 20 years. While a weakened, or "preconditioned," vortex is more likely to break down, it is not a necessary condition for a subsequent SSW to occur [*Fairlie et al.*, 1990].

3.1. Synoptic Overview Preceding the Merger of Anticyclones

[17] To lay the framework for the case study, Figure 3 shows ψ on the 2000 K isentropic surface for 4, 9, 13, and

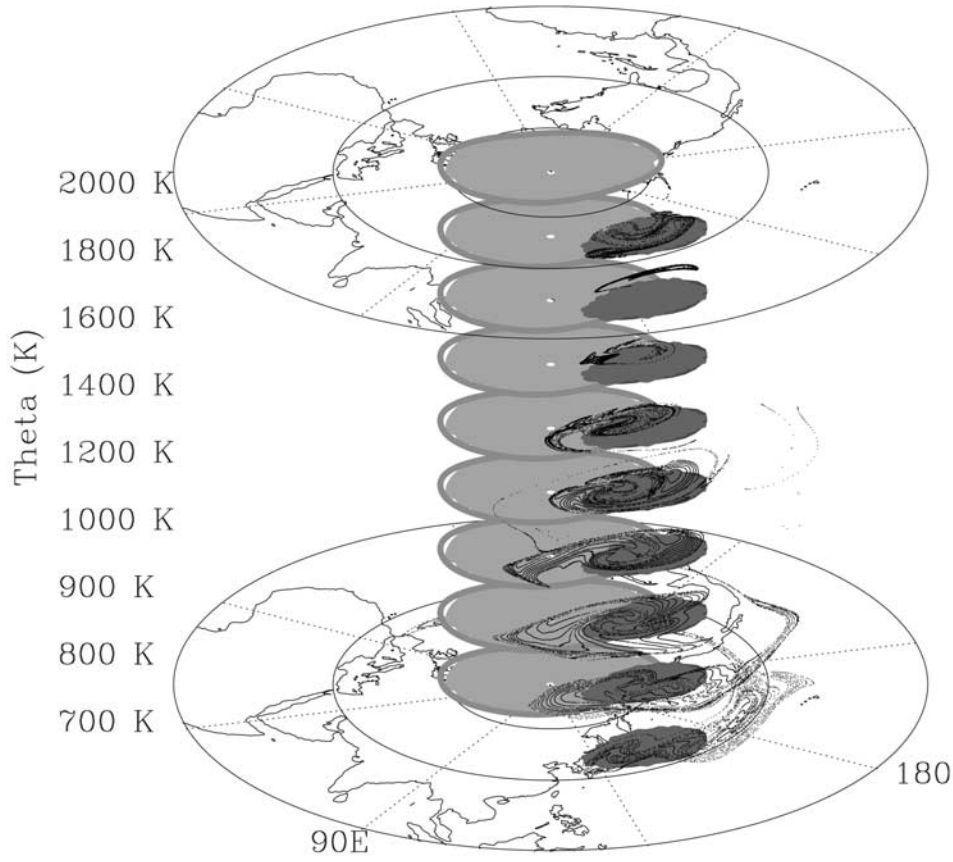

Figure 2. Arctic vortex and Aleutian High edges contoured on 9 overlapping polar stereographic projections on 12 January 2000. The vertical range is from 700 to 1600 K (20–1.5 hPa, or 26–42 km). The Arctic vortex is filled in grey. Material lines (dark contours) are initialized 5 days earlier inside the AH.

17 February, 1999. Thick contours represent the edges of the Arctic vortex and anticyclones. Grid points with negative PV are shown as solid circles. Only negative PV poleward of 10°N is shown (near the equator anomalous PV is common). The anticyclone in the subtropical Atlantic is quite mobile while the anticyclone situated over the North Pacific is comparatively stationary. The presence of the anticyclones distorts the shape of the Arctic vortex, which extends equatorward of 40°N over North America on 4 February 1999 (Figure 3a). A streamer of negative PV extends from the tropical Eastern Pacific poleward and eastward between the mobile anticyclone and the elongated Arctic vortex. This streamer is air that was recently in the SH and is being transported across the Equator at the longitude where the Arctic vortex is furthest from the pole. The cross equatorial advection of SH air takes place down to 900 K, nearly 20 km lower, thus the vertical structure of the displaced SH air is that of a sheet. In this case, the sheet of SH air does not tilt in the vertical, however, it extends further poleward with altitude.

[18] Over the next 5 days the orientation of the Arctic vortex twists 45° counterclockwise, the mobile anticyclone moves 90° eastward and 15° poleward, and the AH retrogrades 45° and weakens (Figure 3b). Counterclockwise rotation of an elongated Arctic vortex is often observed in conjunction with a poleward and eastward-moving anticyclone. SH air is continuously advected poleward in the PNJ region between the vortex and the mobile anticyclone and negative PV values are observed as far north as 50°N. On 13 February (Figure 3c) the structure of the streamer remains well defined and SH air begins to accumulate inside the core of the mobile anticyclone. On 17 February (Figure 3d) the mobile anticyclone merges with the retrogressing AH. While these anticyclones are deep structures, present down to 500 K (30 km lower), on this day they only merge in the 1400–2000 K layer, approximately 10 km below the 2000 K surface shown here.

3.2. Evolution of Vortices During a Major Midwinter Warming

[19] Figure 4 illustrates the evolution of the Arctic vortex (black) and anticyclones (grey) on 8 select days following the merger of anticyclones in the upper stratosphere on 17 February 1999. The vertical dimension in the figure is potential temperature, ranging from 500 to 2000 K. Values of potential temperature are on the left and the hemispheric averaged height of each isentropic surface is to the right. Notice that the height of isentropic surfaces slightly varies from day to day. This time series of vortex "objects" provides a 3-D view of the evolution of the structure of the Arctic vortex and the AH in the stratosphere. Examples of the Arctic vortex illustrated in similar ways include those

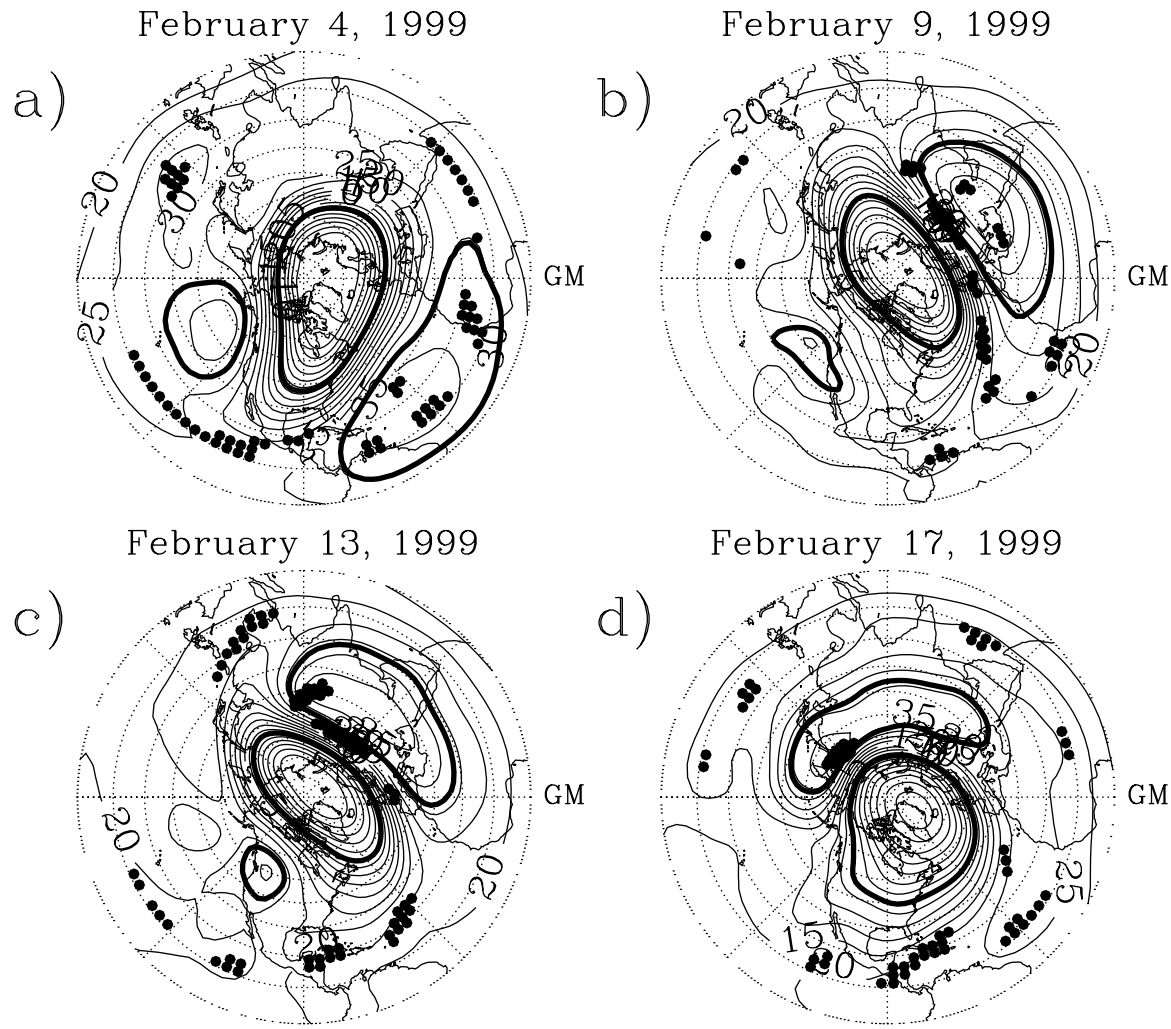

Figure 3. Northern Hemisphere stream function on the 2000 K isentropic surface. Thick contours represent the edges of the Arctic vortex and anticyclones. Filled circles are grid points with negative PV.

of *Manney and Zurek* [1993], *Dameris and Grewe* [1994], *Norton and Carver* [1994], *Manney et al.* [1999], *Waugh and Dritschel* [1999], and *Polvani and Saravanan* [2000].

[20] In the first 3 panels the view is from Indonesia. Figure 4a on 17 February shows the structure of the anticyclone merger above 1400 K (39 km or 3 hPa). Below 1200 K the AH spirals downward and eastward toward North America while the mobile high over the Tibetan plateau is more barotropic and less deep. The structure of the anticyclone pair at this time can be thought of as an upside down and twisted "Y." Above 1000 K the Arctic vortex tilts slightly westward with increasing altitude. By 20 February (Figure 4b), the two anticyclones have merged down to the 1200 K potential temperature surface. Below the 1200 K level the anticyclones do not merge and the distance between the anticyclones increases downward. Since the anticyclones only merge in the 1200–2000 K layer, this "upper regime" behaves in a disconnected manner compared to levels below 1200 K (the "middle regime"). On this day, the AH has moved poleward in the "upper regime" displacing the Arctic vortex toward the North Atlantic. The strong anticyclonic circulation advects polar vortex air equatorward and toward the west in the PWB process. In the "middle regime," theta surfaces descend ≈2 km and temperatures rise over 20 K since 17 February. The intensifying anticyclones "pinch" the weakening polar vortex which is situated between them. In a "lower regime" below 600 K (23 km or 30 hPa), the Arctic vortex is elongated with troughs over Europe and East Asia.

[21] From 13 to 22 February the maximum temperature at 2000 K, located between the mobile anticyclone and the polar vortex, increased by 35 K while the minimum height of the 2000 K surface, displaced slightly to the west of the temperature maxima, descended 1.7 km. By 24 February (Figure 4c) the structure of the vortex is exceedingly distorted. In fact, the vortex is completely entwined around the AH. Above 1200 K, PWB wraps vortex air 180° around the equatorward flank of the AH. The area of the vortex continues to decrease from 800 to 1000 K as the surrounding anticyclones move together. In the "lower regime" the vortex remains elongated. Ridges develop over central Asia and Alaska and act to "pinch" the vortex into 2 centers of low pressure, one over the Arctic Ocean and the other over Siberia.

[22] On 25 February (Figure 4d), the perspective is from the Arabian Sea. This gives a clearer view of the vortex division that occurs near 28 km. Above 1000 K the

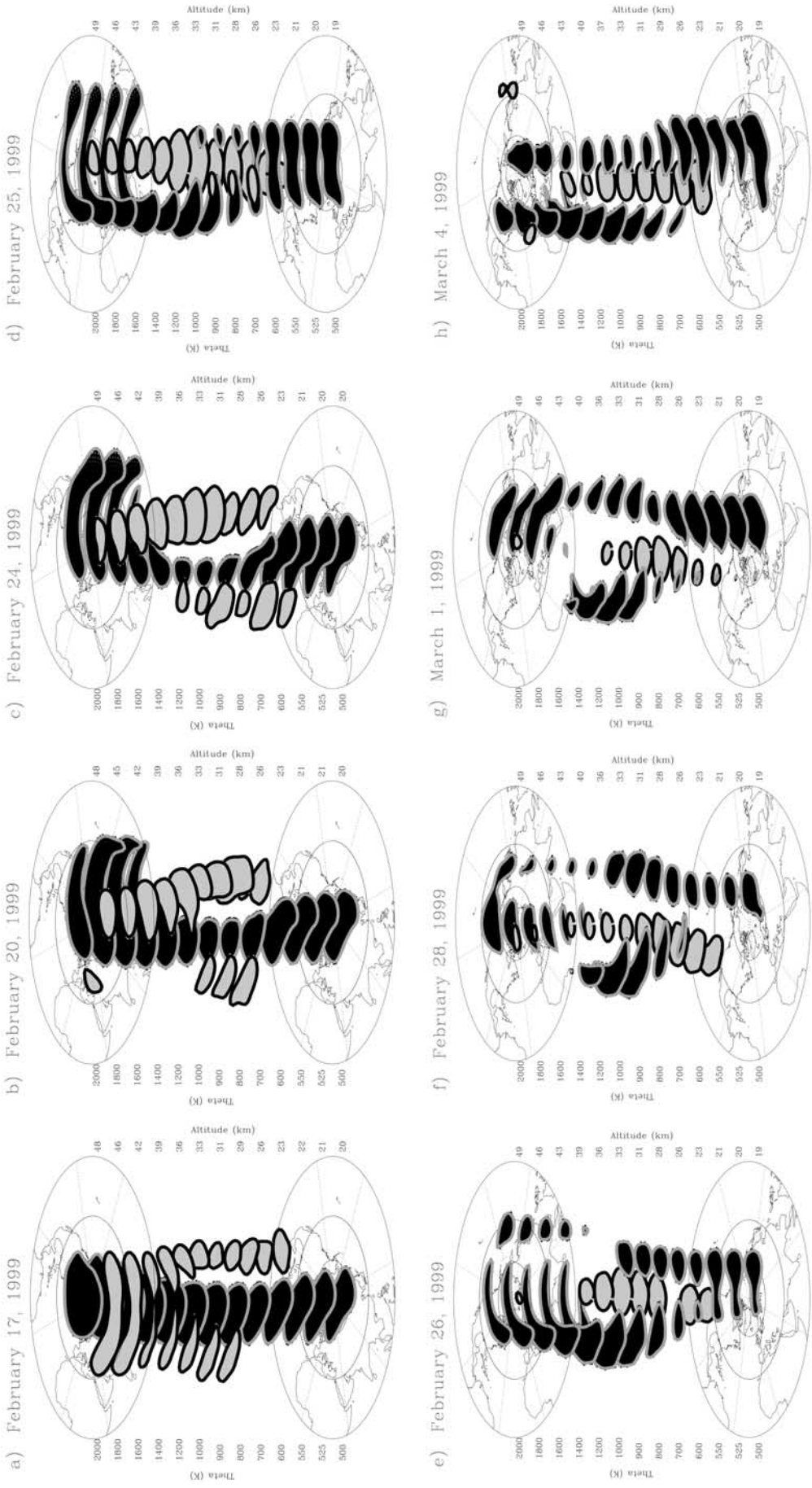

Figure 4. Three-dimensional representation of the Arctic vortex (black) and anticyclones (grey) from 500 to the 2000 K isentropic surface (20–45 km) on (a) 17 February, (b) 20 February, (c) 24 February, (d) 25 February, (e) 26 February, (f) 28 February, (g) 1 March, and (h) 4 March 1999. The view in panels (a)–(c) is from Indonesia. The view in panels (d) and (e) is from the Arabian Sea and in panels (f) and (h) is from Africa.

amplitude of PWB is so extreme that the vortex is stretched into a crescent shape. The structure of the vortex at these altitudes on this day resembles conditions on 16 December 1998 [*Manney et al.*, 1999, Figure 6]. The anticyclone previously designated the AH is now located over the pole. Below 1000 K the polar vortex further elongates and splits into two lobes in the 800–1000 K layer. From 20 to 50 km, the Arctic vortex is completely twisted around the AH such that at 20 km the vortex is in the eastern hemisphere and the AH is in the west while at 50 km the opposite is true.

[23] On 26 February (Figure 4e), the Arctic vortex sheds a cyclonic eddy above 1200 K. Meanwhile, the "unzippering" of the polar vortex extends down to 600 K. On this day the Arctic vortex is divided into 3 distinct air masses: the main vortex over the Greenwich Meridian (GM) that spirals westward with altitude in the 700–2000 K layer and continues to support PWB, the cyclonic eddy from 1000 from 2000 K near the east coast of Asia, and a cyclonic lobe over Siberia below 1000 K. The 2 anticyclones merge and the resulting anticyclone tilts across the pole with altitude. This anticyclone is not identified on some levels due to the algorithms limitation imposed by the maximum longitudinal width criteria. In addition, the area of anticyclones very close to the pole is underestimated since the algorithm stops at the last streamline that does not encircle the pole. This explains why the area of the anticyclone decreases with altitude in Figures 4d and 4e. This limitation will be addressed in subsequent versions of the algorithm.

[24] On 28 February (Figure 4f), the maps are further rotated eastward so that the view is from Africa. What remains of the Arctic vortex is complicated. The cyclonic eddy is advected westward over the Siberian lobe and the two merge in the vertical. At the same time, what was previously referred to as the "main vortex" over the GM sheds a second cyclonic eddy off the coast of North America above 900 K (30 km or 7 hPa). At this point it is not clear which air mass is the "main vortex." Note that the area of the anticyclone is severely underestimated on levels where it is located very near to the pole.

[25] By 1 March (Figure 4g), the second eddy merges into the Siberian lobe as the first eddy did. This reduces the number of separate vortex air masses to 2. The original "main vortex" extends downward, its base supported by a cutoff low over Greenland. The anticyclone remains firmly established over the pole. Unfortunately, the full structure of the anticyclone is not captured. In reality, it is a broad circulation and is continuous through all altitudes shown in the figure.

[26] By 4 March (Figure 4h), both vortex air masses are advected westward around the anticyclone, which has weakened but remains over the pole. By 7 March the vortex begins to recover above 1400 K. Re-establishment continues downward and on 27 March it is a cylindrical shape through all levels. This detailed case study illustrates that the vortex marker algorithms function quite well in a challenging complex situation.

4. Seasonal Mean Frequency

[27] Seasons are given by March–April–May (MAM), June–July–August (JJA), September–October–November (SON), and December–January–February (DJF).

4.1. Zonal Mean Structure

[28] Seasonal zonal mean frequencies of polar vortices and anticyclones provide a broad overview of their structure in latitude and altitude. In Figure 5 zonal mean seasonal polar vortex frequency is contoured. Westerly zonal mean zonal wind ($\overline{U}$) is shaded and easterlies are dashed in the background to show the relative location of the polar vortices with respect to the westerly jets. Polar vortices are identified to varying degrees in fall, winter, and spring but not in the summer above 600 K.

4.1.1. The Arctic Vortex

[29] In the NH fall (Figure 5a), westerlies return in the beginning of September and the Arctic vortex forms from the top down [*Waugh and Randel*, 1999]. This accounts for the increase in vortex frequency with altitude. The Arctic vortex is identified over 80% of the time over the pole above 1100 K and over 60% of the time at all altitudes poleward of 70°. The 3-D structure of Arctic vortex frequency in fall (not shown) reveals that the vortex is centered over the pole at all altitudes. Frequency decreases equatorward to 10% near 50° N and 1% near 40° N. This meridional gradient represents zonal asymmetry and variability and is colocated with the PNJ at the vortex edge. Vortex frequency broadens into the upper stratosphere since the vortex is larger at these altitudes (as will be shown later). NH winter polar vortex frequency (Figure 5b) has a similar structure as in fall. Frequency exceeds 80% at all altitudes over the pole. Meridional gradients in vortex frequency from 50° to 70° N are weaker because the Arctic vortex exhibits more variability in winter than in fall. In NH spring (Figure 5c), an Arctic vortex is identified only 20–30% of the time over the pole. This dramatic decrease from winter to spring is due to the final warming, or decay of the vortex, which happens between March and May. In JJA (Figure 5d), zonal mean easterlies above 500 K are associated with the summer anticyclone.

4.1.2. The Antarctic Vortex

[30] Antarctic vortex frequency is notably different from the Arctic vortex. In SH fall (Figure 5c), the polar vortex is present 10% more often over the pole than in the NH (compare contours in the SH Figure 5c with NH Figure 5a) as formation occurs earlier. As in the NH, in SH fall (Figure 5c), Antarctic vortex frequency increases with altitude (exceeding 90% above 1400 K) due to formation beginning in the upper stratosphere *Waugh and Randel* [1999], however, the vertical gradient in vortex frequency is smaller because formation of the Antarctic vortex occurs more rapidly. Larger meridional gradients reflect increased zonal symmetry compared to in the Arctic. In SH winter (Figure 5d), the Antarctic vortex is present all the time poleward of 80° S, 15% more often than in the Arctic (compare contours in the SH Figure 5d with NH Figure 5b), because the Antarctic vortex always encircles the pole. As in the fall, meridional gradients of Antarctic vortex frequency are larger than in NH fall due to the quasi-stationary latitude of the PNJ. The zonal mean PNJ reaches speeds in excess of 85 m/s, $\approx$1.8 times that observed in the Arctic winter. The Antarctic vortex typically persists over a month longer than in the Arctic *Waugh and Randel* [1999] and for this reason springtime vortex frequency is larger (compare SH Figure 5a to NH

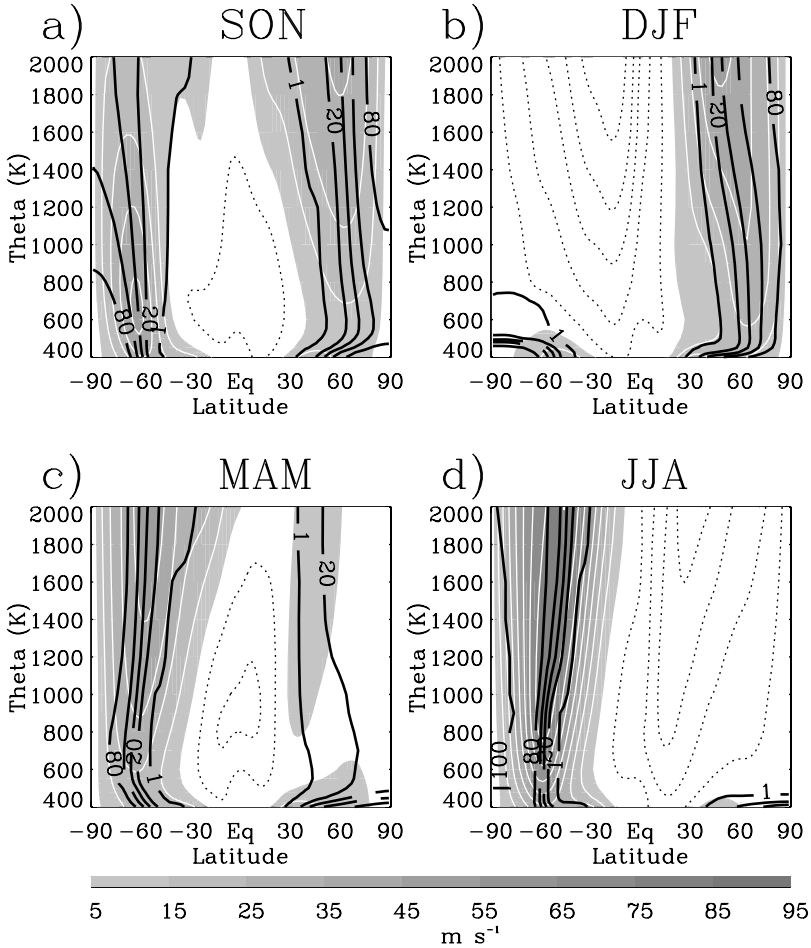

Figure 5. Latitude-altitude sections of average zonal mean zonal wind (westerlies shaded, easterlies dashed) and polar vortex frequency (thick contours) from 1991 to 2001 during (a) September–October–November (SON), (b) December–January–February (DJF), (c) March–April–May (MAM), and (d) June–July–August (JJA). Wind contour interval is 5 m/s. Frequency contours are at 1%, 20%, 40%, 60%, 80%, and 100%.

Figure 5c). Antarctic vortex frequency decreases with altitude since the vortex first decays in the upper stratosphere. In DJF (Figure 5b) zonal mean easterlies above 700 K (26 km or 15 hPa) are associated with the summer anticyclone.

4.1.3. Arctic Anticyclones

[31] Zonal mean seasonal anticyclone frequency is shown in Figure 6. Zonal mean anticyclone frequency maximizes in regions of strong anticyclonic shear of the zonal mean zonal wind $f\left(d\overline{U}dy\right) < 0$. In the Arctic, axes of maximum anticyclone frequency tilt poleward from the subtropical upper troposphere to at least 700 K in all seasons. These axes represent the upward extension of monsoon anticyclones, which tilt poleward and merge zonally with altitude [*Hitchman et al.*, 1997]. In NH fall (Figure 6a), anticyclones are not observed poleward of 70° (and less than 5% of the time poleward of 50°N) due to the establishment of the Arctic vortex (compare to Figure 5a). The pattern of NH fall anticyclone frequency bifurcates with altitude, with extensions both upward and equatorward. Frequency decreases with altitude from 10% at 700 K to 1% at 2000 K.

[32] From fall into winter (Figure 6b), the PNJ intensifies and $d\overline{U}/dy$ increases and shifts poleward (compare Figure 6a to Figure 6b). During this time, anticyclone frequency increases 5- to 10-fold at 50°N from 600 to 1100 K and from the Equator to 45°N above 1300 K. An interesting point to notice is the deep region from 65° and 85°N where anticyclones occur (albeit less than 5% of the time) despite cyclonic $d\overline{U}/dy$. This is due to the chronic displacement of the Arctic vortex toward the GM which gives way to a region of local anticyclonic shear near the Date Line. This is the climatological location of the AH at 10 hPa [*Harvey and Hitchman*, 1996].

[33] Northern spring (Figure 6c) is characterized by a marked decrease in PNJ speed and NH anticyclone frequency. The zone of anticyclonic $d\overline{U}/dy$ migrates equatorward as does anticyclone frequency. The only latitude band where anticyclone frequency increases from winter to spring is poleward of 70°N. This is during the final warming when anticyclones are often located very close to the pole.

4.1.4. Antarctic Anticyclones

[34] As in the NH, in the lower stratosphere monsoon anticyclones are observed to tilt poleward with altitude from

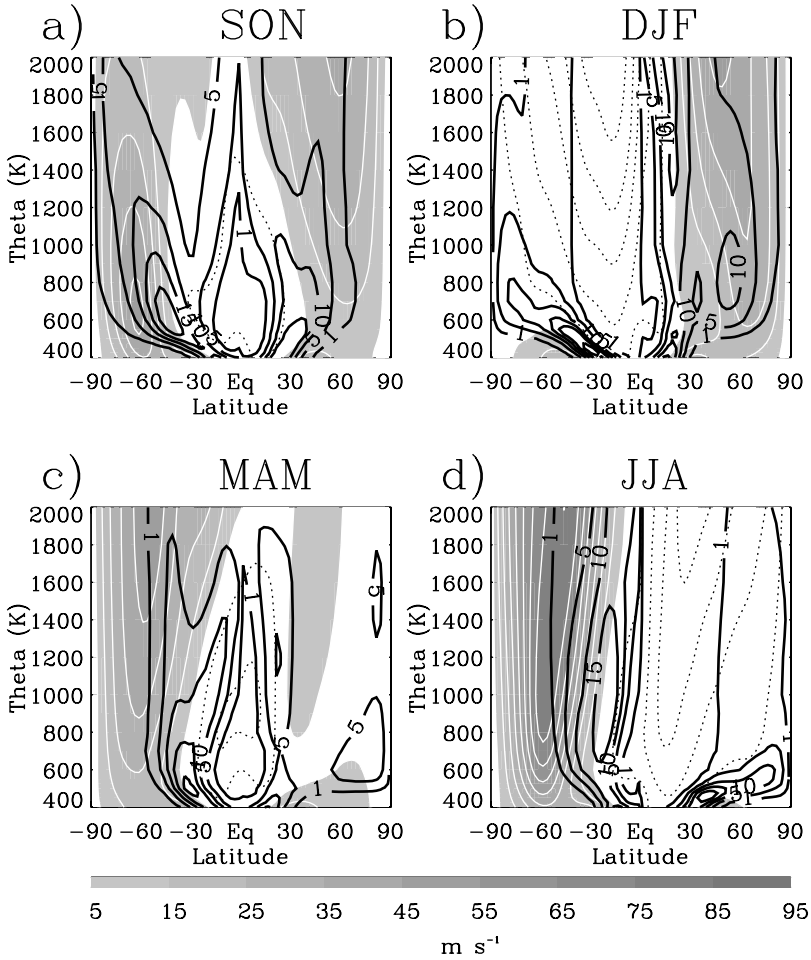

Figure 6. As Figure 5 for anticyclone frequency contoured at 1%, 5%, 10%, 15%, and 20%.

the subtropical tropopause region year-round. In SH fall, the zonal mean structure of anticyclone frequency is similar to NH fall (compare SH Figure 6c with NH Figure 6a). The axis of anticyclone frequency divides with altitude, extending both upward and tilting equatorward. Both regions are coincident with anticyclonic $d\overline{U}/dy$. In SH fall, anticyclones are not present on the poleward side of the westerly jet. This is because the Antarctic vortex is strengthening over the pole and is not a result of a limitation in the algorithm. In SH winter (Figure 6d), $d\overline{U}/dy$ and anticyclone frequency differ from in NH winter. The SH PNJ is stronger and larger and the stable Antarctic vortex effectively eliminates anticyclones poleward of 50°S.

[35] Extratropical anticyclones in the SH occur most often in spring [*Lahoz et al.*, 1996]. The axis of maximum anticyclone frequency tilts poleward with altitude through the depth of the stratosphere. This is a result of the weakening of the Antarctic vortex during this time period, especially in the upper stratosphere. Notice that poleward of 60° S anticyclones occur despite background cyclonic $d\overline{U}/dy$. As in NH winter, the Antarctic vortex is displaced during the SH spring and is accompanied by the quasi-stationary anticyclone referred to here as the "Australian High" (hereafter AUH). Because high latitude anticyclone frequency is largest in the Arctic during winter and in the Antarctic during spring, henceforth we focus on this subset of the climatology.

4.2. Structure in Longitude

[36] Figure 7 is a longitude-altitude section that shows the zonal structure of anticyclone (shaded and light contours) and polar vortex (heavy contours) frequency from 1991 to 2001. Frequencies are averaged in the latitude band from (a) 50–60°N in DJF and from (b) 50–60°S in SON. These latitude bands are chosen to examine the zonal structure of the anticyclone frequency maxima in the SH in Figure 6a and in the NH in Figure 6b. Axes of maximum anticyclone frequency are dotted. The zonal structure is remarkably similar in both hemispheres, with maxima of 40% near 800 K (29 km or 10 hPa) and the Date Line. Likewise, in both hemispheres maxima in anticyclone frequency decreases and tilts westward with altitude. In the NH this structure represents the AH [e.g., *Harvey and Hitchman*, 1996, Figure 9a; *Yoden et al.*, 1999, Figure 10; *Pierce et al.*, 1993, Figure 18] and in the SH is the AUH. The NH frequency maxima is colocated with maximum ozone [*Harvey and Hitchman*, 1996] due to the ozone source being in the tropics where PV is closer to zero. This colocation in the SH is documented in a separate manuscript in preparation. The zonal structure of anticyclone frequency in the subtropics (not shown) is similar in both hemispheres, with maximum anticyclone

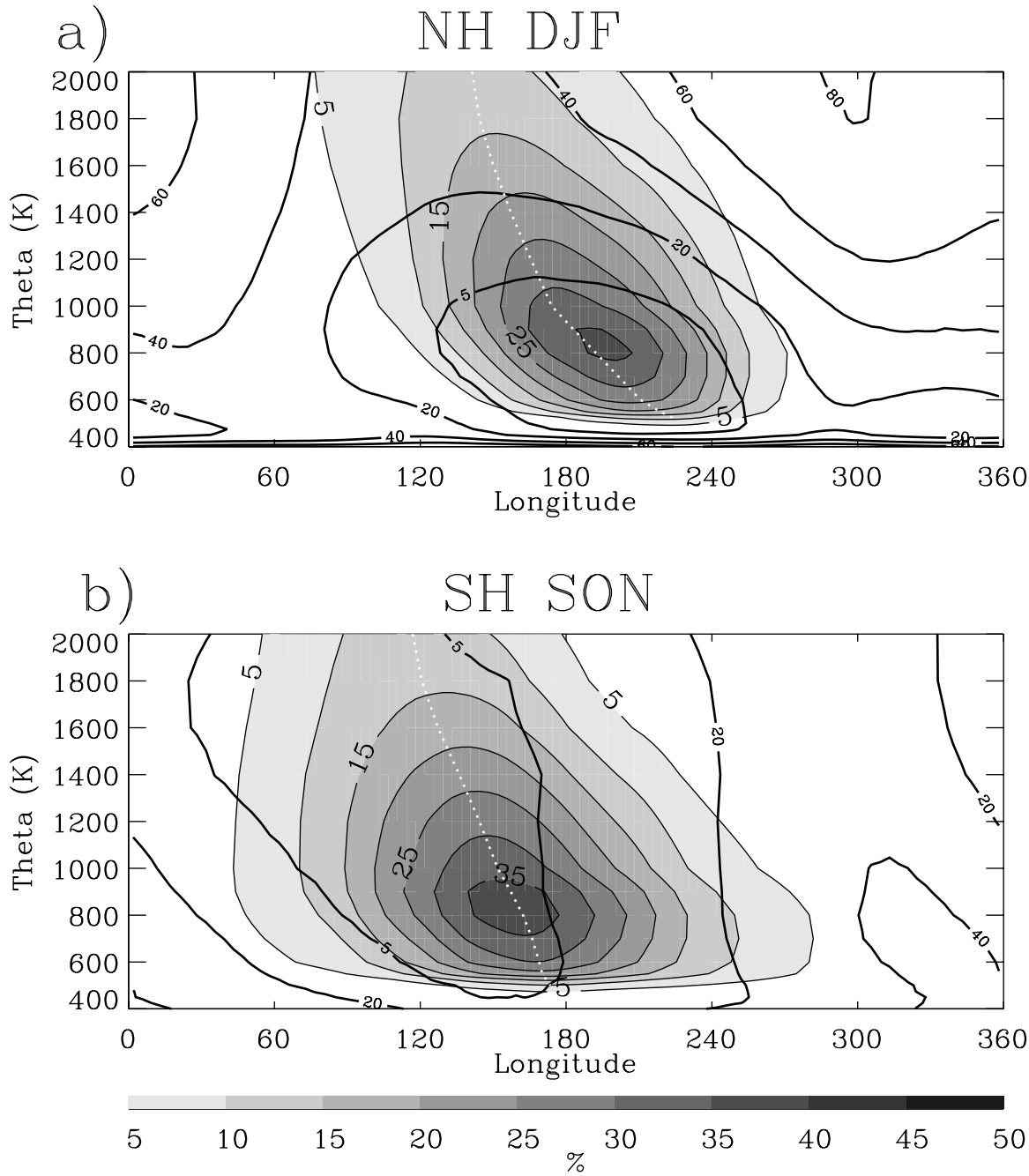

Figure 7. Longitude-altitude section averaged from 50° to 60° of anticyclone frequency (shaded) and polar vortex frequency (contoured) from 1991 to 2001 in the (a) Northern Hemisphere winter and (b) Southern Hemisphere spring. Polar vortex frequency is contoured every 20%. Axes of maximum anticyclone frequency are dotted.

frequency above 1000 K near 300° longitude. However, twice as many subtropical anticyclone are identified in the NH. Sweeping poleward from low latitudes in both hemispheres the location of subtropical frequency maxima moves downward and eastward, eventually merging with the westward tilting frequency maxima at high latitudes.

4.3. Structure in Latitude

[37] Figure 8 is a latitude-altitude section taken along the westward-tilting dotted lines in Figure 7. The longitudes sampled correspond to the peak in the longitudinal frequency distribution. Because this cross section is not averaged over 10°, as in Figure 7, larger frequencies are observed.

[38] In SH fall (Figure 8a), an anticyclone is present over 50% of the time at 170°E, 50°S, and 600 K. The axis of maximum anticyclone frequency tilts poleward with altitude from this point to 80°S at 2000 K. In the upper stratosphere, anticyclones are near the pole during the decay of the Antarctic vortex. Similarly, in NH winter (Figure 8b), an

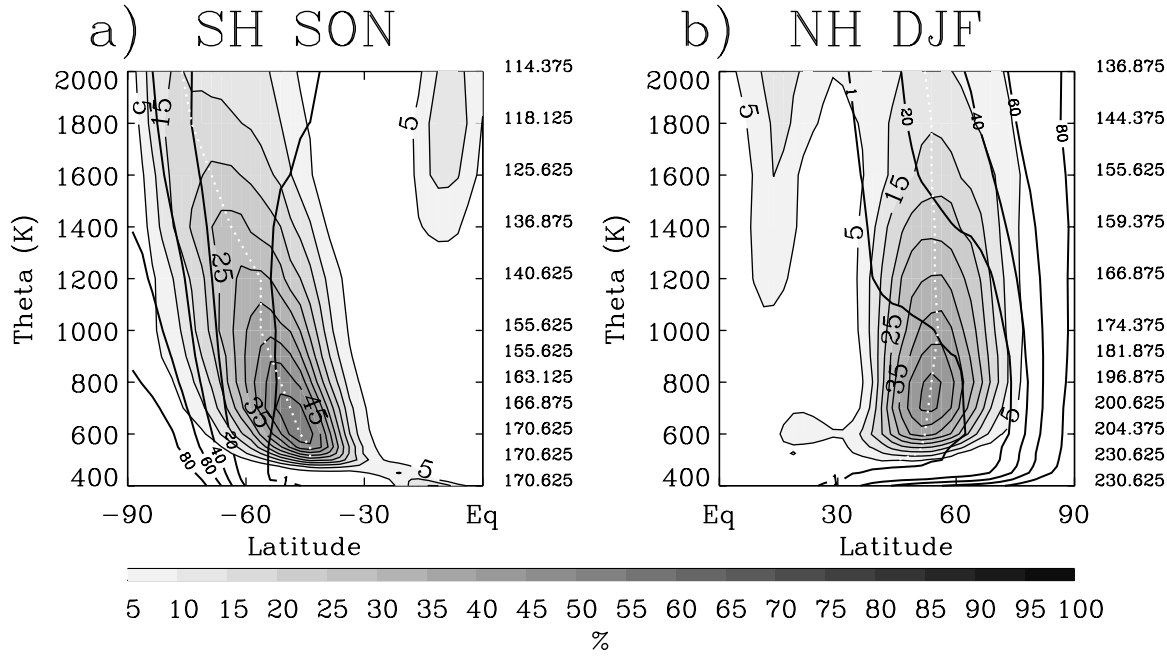

Figure 8. Westward tilting latitude-altitude section along the axes of maximum anticyclone frequency (dotted lines in Figure 4) of anticyclone frequency (shaded) and polar vortex frequency (contoured) from 1991 to 2001 in the (a) Southern Hemisphere spring and (b) Northern Hemisphere winter. At each altitude, the longitude is shown to the right of the figure. Polar vortex frequency is contoured every 20%. Axes of maximum anticyclone frequency are dotted.

anticyclone is present nearly 50% of the time at 200°E, 50°N, and 800 K. The axis of maximum anticyclone frequency tilts less than 5° poleward through the depth of the stratosphere. This is a result of the Arctic vortex being strong and intact through February [*Waugh et al.*, 1999] while the Antarctic vortex is weak in the upper stratosphere in SH spring. Regions where polar vortex and anticyclone frequencies overlap represent PWB, where vortex material wraps around the equatorward flank of anticyclones. The size of this overlapping region increases with altitude, consistent with the amplification of PWB toward the stratopause [*Waugh and Dritschel*, 1999; *Polvani and Saravanan*, 2000].

4.4. 3-D Structure

[39] Figure 9 shows a 3-D perspective of NH anticyclone and Arctic vortex frequencies during DJF on the 800 K, 1200 K, and 1600 K potential temperature surfaces. These surfaces are near 29, 36, and 42 km and 10, 4, and 1.5 hPa, respectively. The axis of maximum Arctic vortex frequency exceeds 92% at all altitudes. This axis is displaced toward 60° E at 800 K and tilts westward and equatorward with altitude, placing it at the GM at 1600 K. In the western hemisphere, the meridional gradient in vortex frequency decreases with altitude. This 3-D depiction more clearly illustrates the relationship between cyclone/anticyclone overlap and increased PWB.

[40] At each altitude, there are four distinct maximum in anticyclone frequency. In the subtropics, anticyclones are observed over Central America (290°E, 15°N), Western Africa (340°E, 25°N), and India (75°E, 30°N) 10–35% of the time. These anticyclones appear tied to subtropical landmasses. The maxima in anticyclone frequency over the North Pacific (180°E, 50°N) is the AH and, as stated earlier, is present over 50% of the time at 800 K. As will be shown later, anticyclones that make up these frequency maxima are predominantly quasi-stationary, moving slowly east and west about their central locations. However, several times each winter subtropical anticyclones are observed to move great distances along preferred pathways.

[41] Figure 10 shows SH anticyclone and Antarctic vortex frequency during SON on the 800 K, 1200 K, and 1600 K isentropic surfaces. The Antarctic vortex is displaced toward 330°E and is relatively barotropic. It is present over 90% of the time below 800 K (not shown). Above 800 K, maximum frequency decreases to 55% at 2000 K. This 3-D structure resembles that of a "distorted cone" [*Mechoso et al.*, 1988] and is a result of the Antarctic vortex breaking down first in the upper stratosphere. Reduced meridional gradients in vortex frequency at 225° are a result of PWB.

[42] There are at least two main anticyclone centers on each level connected by a pathway of maximum frequency. The most frequent anticyclone in the SH, the AUH, occurs poleward of Australia (150°E, 60°S) This is the SH counterpart to the AH. In the subtropics, anticyclones are identified near the landmass of South America (300° E, 20°S) 20% of the time. In some years there is a distinct maxima in anticyclone frequency over Africa (1995–1997) while in other years the pattern of anticyclone frequency resembles the climatological mean. The reduction in sub-

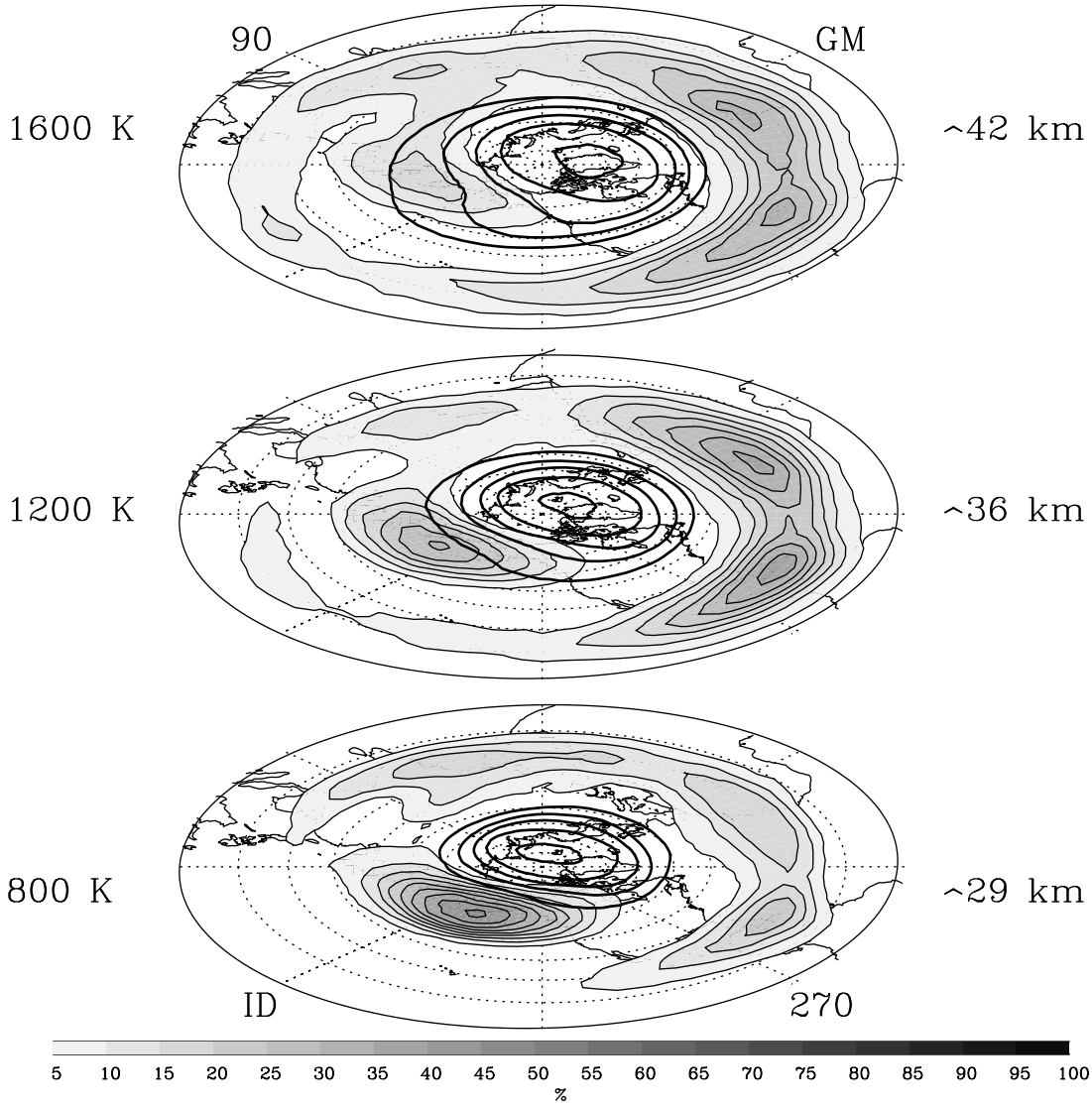

Figure 9. Arctic winter anticyclone (shaded) and polar vortex (contoured) frequencies from 1991 to 2001 on the 800, 1200, and 1600 K isentropic surfaces. The center of each projection is the North Pole, the outer circle is the equator, latitude circles are drawn every 10°, and a polar stereographic map is drawn. Arctic vortex frequency is contoured in 20% intervals beginning at 10%. Anticyclone frequency is shaded every 5% beginning at 5%.

tropical anticyclone frequency compared to the NH and the pathway of maximum anticyclone frequency connecting the two is likely due to "repeating sequences of anticyclogenesis, eastward advection and decay" [*Lahoz et al.*, 1996].

5. Evolution of Polar Vortex and Anticyclone Area

[43] Next we examine the temporal evolution of polar vortex and anticyclone area as a function of potential temperature. Area is calculated in km^2 and then converted into equivalent latitude ϕ_{eq} [*Butchart and Remsberg*, 1986]. ϕ_{eq} is equal to the area enclosed by latitude circles thus larger ϕ_{eq} corresponds to a smaller area. Here, 10 years of ϕ_{eq} time-altitude sections are averaged and the mean evolution of area is shown.

5.1. Polar Vortices

[44] Figure 11 is the climatological evolution of polar vortex ϕ_{eq}. Below 500 K in both hemispheres, polar vortex ϕ_{eq} persists near 60° without a clear annual cycle. As mentioned earlier, this is a result of biases due to the year-round presence of the subtropical jet streams. Therefore, this discussion focuses on altitudes above 500 K.

[45] The Arctic vortex (Figure 11a) forms over the course of about a week from the top down in mid-September. It expands at the same rate at all altitudes until late October, at which time it grows more rapidly in the upper stratosphere. From October through December, the Arctic vortex is typically cone shaped, with area increasing with altitude. The evolution of Arctic vortex area below 900 K is such that area maximizes (ϕ_{eq} = 63°) in late November, then slowly decreases through April and the final warming. These results agree with calculations performed at 700 K

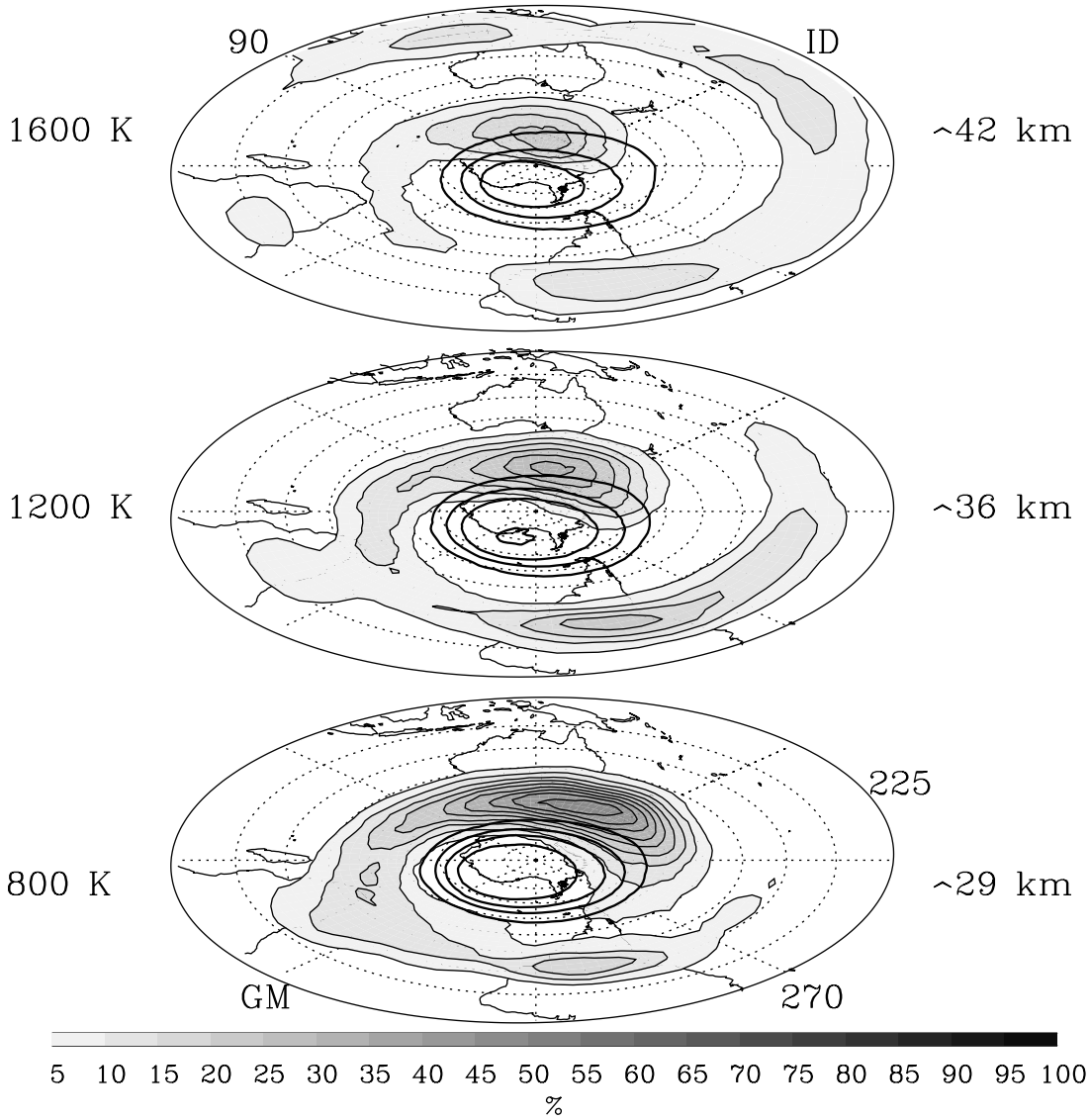

Figure 10. As Figure 9 for the Southern Hemisphere during SON.

by *Waugh* [1997] (compare Figure 11a with his Figure 6a) with the vortex edge defined by fitting an "equivalent" ellipse to the 40–60 ppb N_2O isopleths. Above 900 K, the mean evolution of area does not steadily decrease after reaching a maximum size ($\phi_{eq} < 50°$) in early December. Instead, the evolution has a bimodal structure, with a maximum in early December ($\phi_{eq} = 50°$), a minimum in early February ($\phi_{eq} = 65°$), and a second maximum in March ($\phi_{eq} = 57°$). These findings agree with [*Waugh and Randel*, 1999, Figures 2b and 2d] who note a "bite" out of Arctic vortex ϕ_{eq} during January and February at 1300 K. This midwinter minimum is primarily due to PWB, a process known to weaken the polar vortex [e.g., *McIntyre and Palmer*, 1983] and decrease its area [*Butchart and Remsberg*, 1986; *Pierce et al.*, 1993]. A reduction in polar vortex area in the upper stratosphere results in a more cylindrical shape. Such vertical variations in polar vortex area are known to affect linear and nonlinear wave propagation and breaking [*Waugh and Dritschel*, 1999]. The Arctic vortex decays from the top down in mid to late April. This timing agrees with *Waugh and Dritschel* [1999] (see their Figure 12a) despite there being a large degree of interannual variability (not shown). From June through August the Arctic vortex takes the shape of a small cone from the tropopause to 600 K. The evolution of Arctic vortex area in the lower stratosphere agrees to within a few degrees of equivalent latitude with the results of *Nash et al.* [1996] at 450 K.

[46] Figure 11b shows the climatological evolution of Antarctic vortex ϕ_{eq}. The time axis is shifted so that the winter season is in the middle of the figure. The climatological evolution of Antarctic vortex ϕ_{eq} is smoother than in the Arctic due to less interannual variability. The Antarctic vortex forms in early to mid-March. Following formation, vortex area increases at all altitudes through May, albeit more rapidly above 1000 K. In early June, maximum area ($\phi_{eq} < 50°$, 5° larger than in the Arctic), is observed above 1400 K. This maximum descends such that the time at which the vortex is largest at 600 K is in August. Vortex area decreases gradually from July through October. In

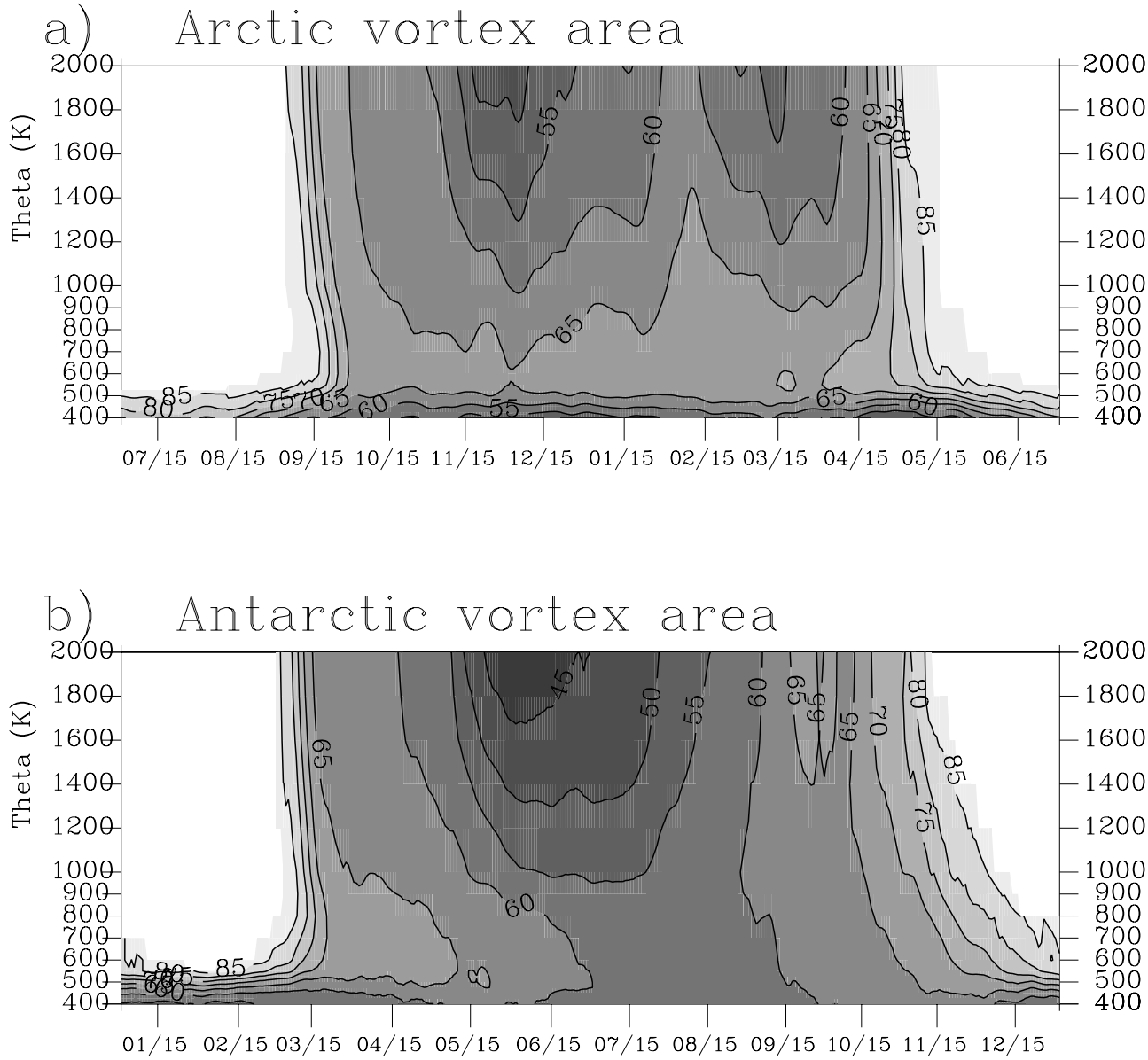

Figure 11. Time-altitude sections of average polar vortex area from 1991 to 2001 in the (a) Northern Hemisphere and b) Southern Hemisphere. Area is expressed in terms of equivalent latitude (ϕ_{eq}). Contour interval is 5°.

November and December, the Antarctic vortex decays from the top down. Compared to the structure of the Arctic vortex in NH summer, from late December through February the Antarctic vortex is a deeper cone with a base 5 times larger. This evolution agrees with *Waugh and Randel* [1999] (compare Figure 11b with their Figure 4b).

5.2. Anticyclones

[47] Figure 12 shows the climatological evolution of anticyclone area in the NH as a function of altitude. In the NH (Figure 12a), anticyclone area increases at all levels in late August, several weeks before the formation of the Arctic vortex. This is likely the time when the summertime circumpolar anticyclone ceases to encircle the pole. At this time anticyclone area is constant with altitude. In early winter (SON), anticyclone area maximizes below 700 K and minimizes above 1000 K such that area decreases with altitude. The minimum in the upper stratosphere occurs when the Arctic vortex is growing while polar vortex area is steady below 700 K (compare Figure 12a to Figure 11a). In mid to late November, when Arctic vortex area plateaus, anticyclone area begins to increase. During December and January, when the Arctic vortex temporarily shrinks, anticyclone area maximizes. The timing of this maximum is consistent with the results of *Harvey and Hitchman* [1996] who found January to be the month of maximum AH frequency at 10 hPa. Above 1000 K in February and March, the same altitude and time where recovery of the Arctic vortex is observed, anticyclone area decreases. During April and May, area is again constant with altitude and decreases more gradually than the rate of increase in August. Anticyclones are identified to some extent year-round below

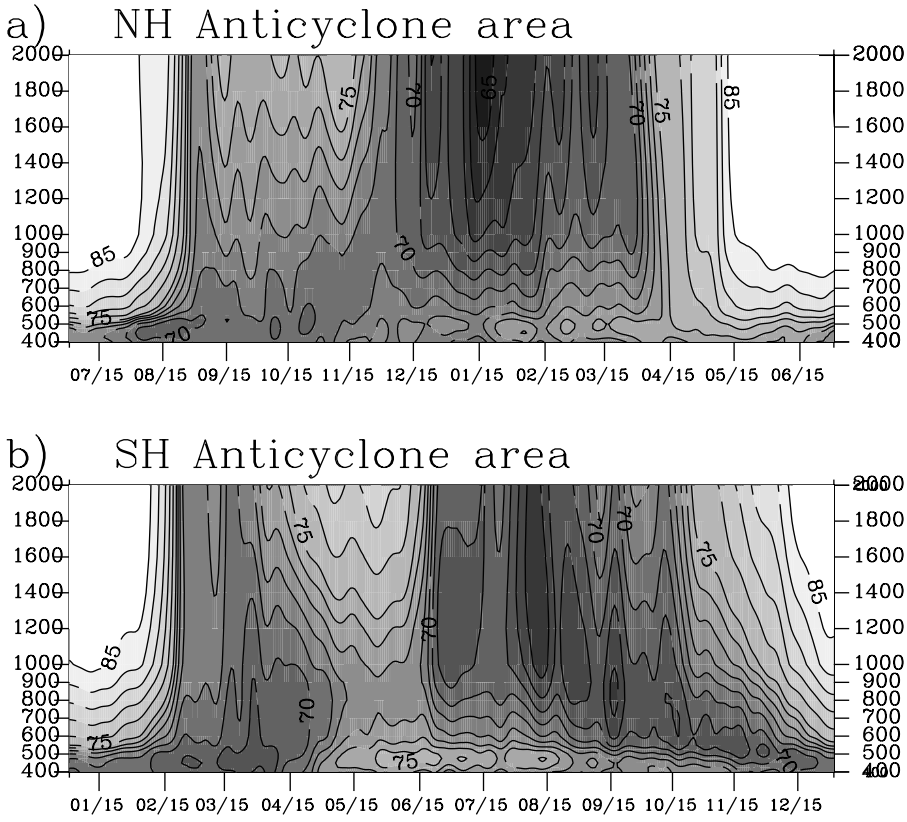

Figure 12. As Figure 11 for anticyclone area. Contour interval is 1° from 65° to 75° and 2° from 75° to 85°.

800 K. There may be a maximum in anticyclone area during the summer if the algorithm identified circumpolar anticyclones however, this circulation may be too broad and weak to have negative $\oint Q$. We leave this investigation as a topic of future study.

[48] Figure 12b shows the evolution of anticyclone area in the SH. Hemispheric similarities are apparent. Anticyclones are present year-round below 1000 K. In February, anticyclone area increases before the Antarctic vortex is established. In early March, when the vortex forms, anticyclone area stops increasing. From mid-March to mid-June, when the Antarctic vortex is expanding, anticyclone area decreases. Throughout the depth of the stratosphere, reduction in anticyclone area is colocated with vortex area increases. Minimum SH anticyclone area in May is four times smaller than in the NH. In mid-June above ≈800 K, following the time that the Antarctic vortex maximizes, anticyclone area rapidly increases. Then from July through September, when vortex area decreases, anticyclone area maximizes. From August through December, this maximum descends from 2000 K to 400 K, lagging the decent of maximum Antarctic vortex area by 2 months. In November and December, anticyclone area decreases gradually, following the breakdown of the Antarctic vortex.

[49] In both hemispheres, the evolution of anticyclone area has the following characteristics. Anticyclones are identified prior to the formation of the polar vortex and persist beyond the final warming. Minimum anticyclone area occurs when polar vortices are growing while maximum anticyclone area is observed when the polar vortices are shrinking. The latter is explained by the relationship between the AH and the AUH with the polar vortices and PWB in that growth of anticyclones promotes PWB which erodes the polar vortices.

6. Daily Movement of Anticyclone Centers at 1200 K

[50] In this section we examine the daily motion of anticyclones on the 1200 K isentropic level. Despite the vertical variation in anticyclone structure, motion on this level is often representative of the 600–2000 K layer.

6.1. Northern Hemisphere

[51] Figure 13 shows the daily movement of individual NH anticylone centers of mass during 9 DJF seasons. Seasonal mean ψ is contoured to provide dynamical context. Movement is determined by comparing the position of centers on the previous and the following day. Anticyclone centers that move less than 10° longitude and 5° latitude are considered quasi-stationary and are represented with squares. Anticyclone centers that are within 45° longitude and 20° latitude but exceed the quasi-stationary distance are considered mobile and are connected with an arrow. Over 80% of anticyclone centers meet one of these two criteria. Anticyclone centers that do not neighbor another center within one day and 45° longitude and 20° latitude are not included in order to eliminate anticyclones that do not display continuity in time or space. Some of the anticyclones that are eliminated may be a result of a

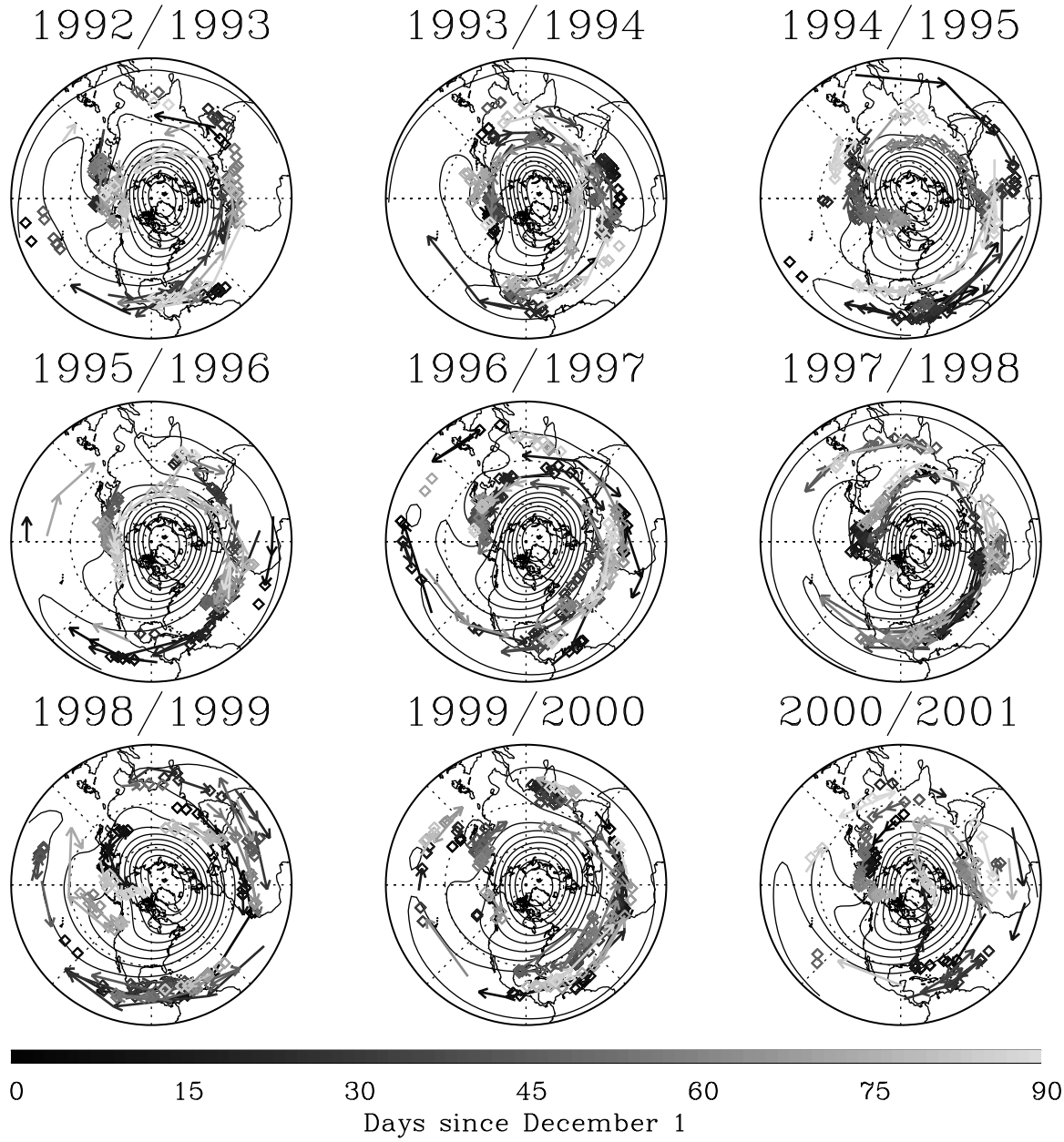

Figure 13. Daily position and movement of Northern Hemisphere anticyclones for each DJF season from 1992 to 2001 on the 1200 K isentropic surface. Contour interval is 10%. See color version of this figure at back of this issue.

circulation temporarily weakening such that the algorithm fails to identify it over its entire lifetime. Anticyclone centers are colored based on elapsed days between 1 December and 28 February. The duration of each color is about a week. It is common for multiple anticyclones to be present on a given day. This occurs when like colored centers are in different places and are not connected to each other. While difficult to detect in this figure, the merger of anticyclones occurs when like colors approach each other. Anticyclones identified near the pole (1994/1995, 1997/1998, 1998/1999, and 2000/2001) are observed during SSWs.

[52] Anticyclones that comprise the four anticyclone frequency maxima (see Figure 9) are often quasi-stationary or slowly vacillate about their central locations. An important consequence of the quasi-stationary AH is that it displaces the Arctic vortex toward lower latitudes that may be sunlit, thus activating chemically processed air, which increases ozone loss [*Degorska and Rajewska-Wiech*, 1996]. Several times each winter an anticyclone can be tracked continuously over great distances. Examples of this long range motion include from India toward the Date Line in 2000/2001, from Africa toward the Date Line in 1992/1993, 1993/1994, 1994/1995, 1995/1996, and 1997/1998, from Central America to Africa in 1992/1993, 1993/1994, 1996/1997, 1997/1998, and 1999/2000, from Central America eastward all the way to the Date Line in 1992/1993, 1997/1998, from India toward Africa in 1998/1999, and from Africa to Central America in 1994/1995. Less frequent paths are observed from Central America and India to the

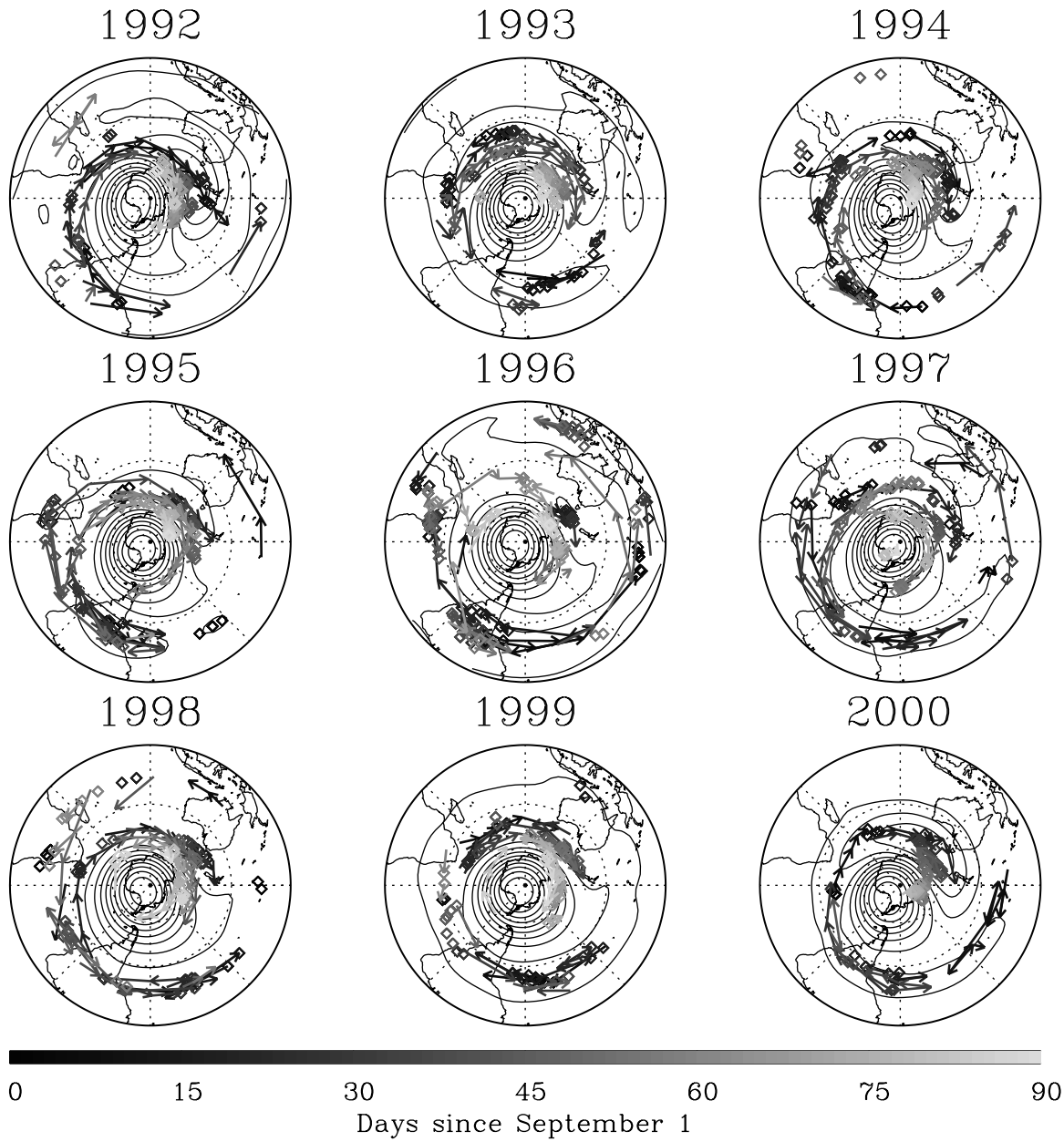

Figure 14. As Figure 13 in the Southern Hemisphere during SON. See color version of this figure at back of this issue.

Pole in 2000/2001. One can see from this list and from a quick inspection of the figure that sustained continuous motion occurs most often from Central America to Africa and from Africa toward the Date Line. In these cases, as an anticyclone moves eastward it also moves poleward. This poleward motion acts to strengthen anticyclonic circulations in the conservation of absolute vorticity. While the causes of anticyclogenesis at low latitudes remains illusive, equatorward displacement of the polar vortex [*Waugh*, 1993] and inertial instability [*Knox*, 1997; *Rosier and Lawrence*, 1999] are suspected to play a role in the propagation of disturbances out of the tropics.

6.2. Southern Hemisphere

[53] Figure 14 shows the daily movement of individual SH anticylone centers at 1200 K during 9 SON seasons. The same distance criteria is used to illustrate the movement of quasi-stationary and mobile anticyclones as in the NH. Anticyclones during southern spring are either quasi-stationary or, almost exclusively, move eastward. The motion of mobile anticyclones is more regular and periodic than in the NH and they can be tracked over longer distances. This suggests that the lifetime of mobile anticyclones in the SH exceeds that in the NH. In particular, the subtropical anticyclone over South America appears to be a region of enhanced anticyclogenesis and the beginning of a pathway for mobile anticyclones. In daily sequences of polar stereographic projections of ψ (not shown), anticyclones are often observed to form in the vicinity of South America and then migrate continuously eastward around the Antarctic vortex, past Africa and into the Australian sector. The periodicity of this life cycle is shorter than the life cycle itself. In other

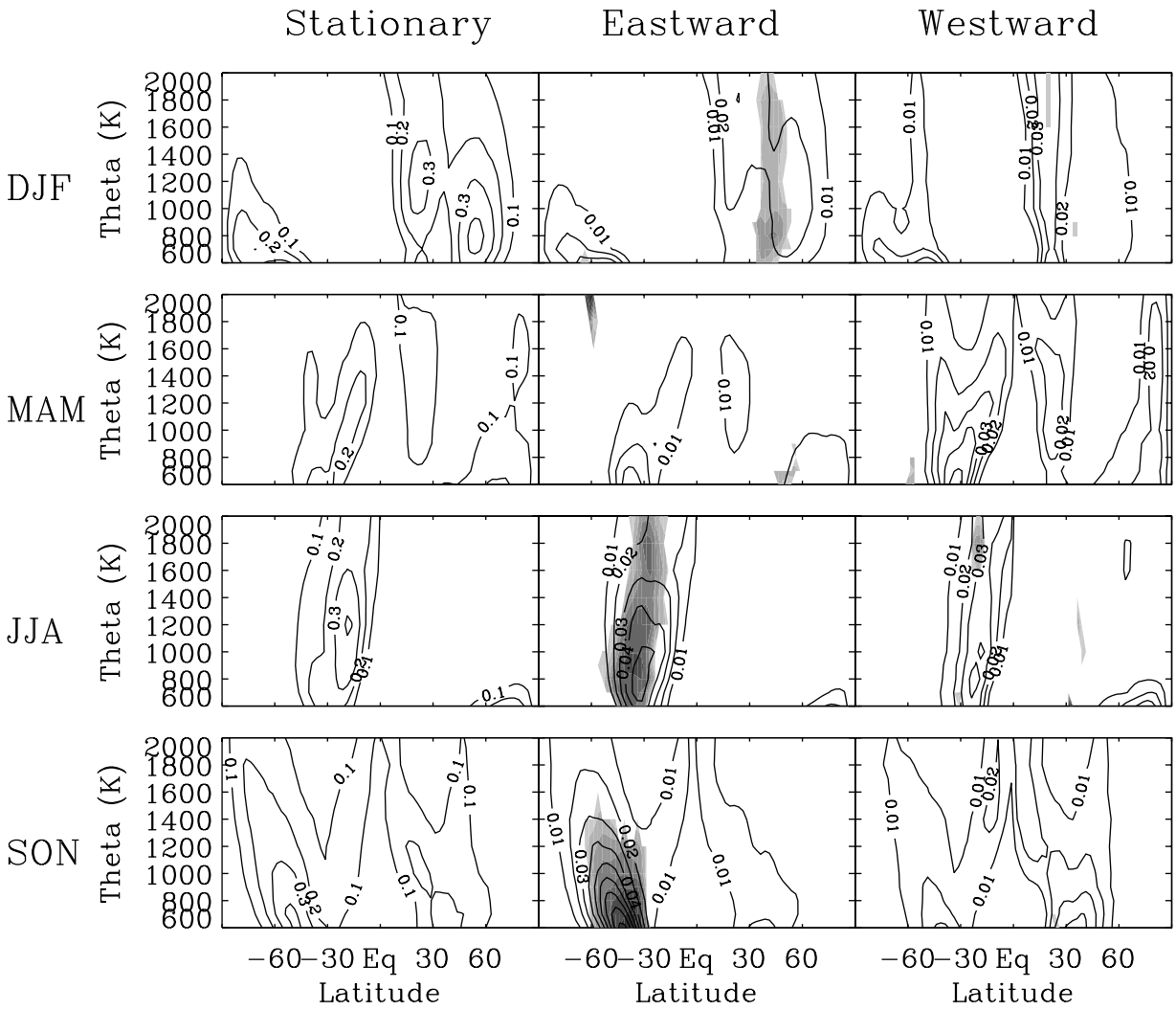

Figure 15. Latitude-altitude sections of anticyclone power spectra. Rows 1–4 are each season. Columns 1–3 are stationary, eastward, and westward components. Shaded areas are where the amplitude of wave 2 exceeds that of wave 1. Contour interval is 0.1 for the stationary waves and 0.01 for the traveling waves.

words, before an anticyclone reaches Australia another high forms over South America and begins moving eastward along a similar track. Hence, there are often two anticyclones present during the breakdown of the Antarctic vortex and the merger of anticyclones is common. Irreversible folding and mixing of air originating inside both anticyclones occurs within the resulting anticyclone following a merger event [*Lahoz et al.*, 1996]. As a mobile anticyclone moves around an elongated polar vortex, the major axis of the polar vortex rotates in the same direction and at the same rate as the motion of the anticyclone. This rotation has been well documented and referred to as an ''eastward traveling wave 2'' [e.g., *Mechoso and Hartmann*, 1982; *Shiotani et al.*, 1990]. Once anticyclones reach Australia their motion becomes quasi-stationary. As the area of the Antarctic vortex decreases, anticyclones encircle higher latitudes, eventually moving over the pole during the final warming. This is in contrast to the somewhat irregular behavior of mobile anticyclones in the NH. This frequent and continuous life cycle route has transport and mixing implications [*Pierce and Fairlie*, 1993]. As in the NH, the AUH displaces the Antarctic vortex from the pole and its growth and decay likely influences the ozone budget.

7. Quasi-Stationary Versus Travelling Anticyclones

[54] In this section, the range of amplitude-weighted anticyclone phase speeds are computed on each potential temperature surface. Seasonal time periods of 90 days are used with once-daily data. On each day, level, and latitude anticyclones are spectrally decomposed in longitude for wave numbers 1–6. On each day and for each wave number this results in a latitude-altitude section of spectral coefficients. Seasonal time series of coefficients are then constructed at each latitude and altitude for each wave number. These time series are then spectrally decomposed in time to determine phase speeds. Resolvable wave periods range from 90 days to the Nyquist frequency of 2 days. The

resulting power spectrum is a function of latitude, altitude, wave period, and wave number.

[55] We integrate over wave period and wave number to identify latitudes and altitudes with power in the stationary and traveling components. Wave periods exceeding 30 days are considered stationary. Transient wave periods range from 5 to 22.5 days. Latitude-altitude sections of power spectra are shown in Figure 15. The spectral amplitude of the stationary component is typically 10 times larger than either traveling component. Transient wave periods range from 6 to 20 days depending on season, hemisphere, and altitude.

[56] In NH fall, westward traveling wave 1 anticyclones are observed. In NH winter, quasi-stationary wave 1 (the AH) and eastward moving waves 1 and 2 in mid to high latitudes are accompanied by westward traveling wave 1 anticyclones in the subtropics. In SH fall anticyclones move westward in the subtropics. In SH winter there is no spectral power at high latitudes. Instead, quasi-stationary and westward traveling wave 1 anticyclones and eastward traveling wave 2 anticyclones are observed in the Southern subtropics. The strength and size of the Antarctic vortex does not allow anticyclones to penetrate poleward. However, the SH spring is characterized by quasi-stationary wave 1 and eastward traveling wave 2 in mid and high latitudes. The only situation where the spectral power in wave 2 exceeds that in wave 1 is eastward moving anticyclones during NH winter and SH winter and spring. These results agree with previous studies of the behavior of SH anticyclones [*Mechoso et al.*, 1988, 1991; *Farrara et al.*, 1992; *Lahoz et al.*, 1996].

8. Summary and Conclusions

[57] In this paper we present a new algorithm which is used to identify anticyclones and polar vortices. Vortex edges are identified by integrating Q around ψ isopleths. Discrete regions dominated by rotation are identified from 330 K to 2000 K over a 10-year period (1991–2001). The daily evolution of identified anticyclones is shown during February and March 1999. During this time, the algorithms perform well during both an anticyclone merger event and a midwinter breakdown of Arctic vortex. Emphasis is placed on characterizing the structure of anticyclones and polar vortices as ''objects'' associated with distinct circulations and enclosed air masses.

[58] Seasonal mean zonal mean frequency of polar vortices shows their persistence at each latitude and altitude and their location relative to zonal mean westerly jets. The Antarctic vortex forms more rapidly, lasts longer, and is less variable than the Arctic vortex. Anticyclones occur where there is background anticyclonic zonal mean wind shear. In all seasons from 330 to 700 K anticyclones tilt poleward out of the tropics and subtropics. Above 700 K, midlatitude and extratropical anticyclones are observed most often in NH winter and SH spring. The longitudinal structure from 50° to 60° during NH winter and SH spring show that, in both hemispheres, anticyclones and polar vortices tilt westward with altitude. Maximum anticyclone frequency (35%) and minimum polar vortex (10%) frequency is observed near the Date Line. Maximum polar vortex frequency is observed near 300°E and increases with altitude (70%). Latitude altitude cross sections along the axes of maximum anticyclone frequency show that anticyclones in the Southern spring also tilt poleward, while NH winter anticyclones do not. Anticyclones are observed 50% of the time near 50° and 700 K in NH winter and SH spring. Regions where both anticyclones and polar vortices occur expand with altitude due to increased PWB with height. Analysis in 3-D revealed that, in the NH, anticyclones occur most often over Central America, Western Africa, India, and the North Pacific. In the SH anticyclones are most often near South America, Africa, and poleward of Australia.

[59] The evolution of both Arctic and Antarctic vortex area agrees with results based on elliptical diagnostics [*Waugh and Randel*, 1999]. In both hemispheres, anticyclones are identified prior to the formation of the polar vortex and persist beyond the final warming. In early winter in the upper stratosphere, minimum anticyclone area occurs when polar vortex area is increasing from September to December in the NH and from March to June in the SH. Maximum anticyclone area occurs when the polar vortices are shrinking. This is from December to March in the NH and from July to October in the SH. In the SH, descent of maximum anticyclone area lags the descent of maximum in Antarctic vortex area by 2 months. This lag is due to increased anticyclogenesis as the vortex weakens.

[60] Frequency and anticyclone motion at 1200 K is shown for each NH winter and SH spring. In NH winter, anticyclone motion poleward of 30°N is most often eastward while anticyclones at lower latitudes typically move toward the west. The AH often displaces the Arctic vortex from the pole which is believed to be an important factor that increases ozone loss. The AH and the anticyclone over Central America are often quasi-stationary while motion of the high over Africa is less predictable. The frequency of cross-equatorial advection of PV is colocated with maxima in anticyclone frequency. This appears to be the result of the poleward transport of air across the equator between the polar vortex and mobile anticyclones. In SH spring, anticyclones form in the subtropics near South America and propagate eastward and poleward in a periodic fashion. Before these mobile anticyclones merge with the quasi-stationary anticyclone at high latitudes near Australia another has formed near South America.

[61] Spectral decomposition of the anticyclones is performed to determine the frequency of mobile anticyclones to stationary anticyclones. In NH fall, westward traveling wave 1 anticyclones dominate. In NH winter, quasi-stationary wave 1 (the AH) and eastward moving waves 1 and 2 in mid to high latitudes are accompanied by westward traveling wave 1 anticyclones in the subtropics. In SH fall subtropical anticyclones travel westward. SH spring is characterized by quasi-stationary wave 1 and eastward traveling wave 2 in mid and high latitudes.

[62] This climatology provides new insight into the frequency and location of stratospheric anticyclones, thus expanding the current knowledge of stratospheric dynamics. The formation, growth, and movement of anticyclones in the stratosphere alter the structure of the Arctic and Antarctic polar vortices, the extent of springtime ozone loss, and planetary wave propagation. This work aids in understanding these anticyclone life cycles. Future work includes integrating chemical data into the climatology to determine the role of traveling anticyclones in the transport of con-

stituents. Extension of the climatology into the troposphere is of interest to study trends in cyclone/anticyclone occurrence and duration and the association between cyclones/anticyclones and the transport of smoke, dust, and pollution.

[63] **Acknowledgments.** The authors would like to thank Alan O'Neill and the UK Meteorological Office for producing the analyses. We would also like to thank the Distributed Active Archive Center at the Goddard Space Flight Center for distributing the data. We appreciate the reviewers' comments and suggestions, which improved the quality of this manuscript. M.H.H. was funded by NASA grant NAG-1-2162.

References

Babiano, A., G. Boffetta, A. Provenzale, and A. Vulpiani, Chaotic advection in point vortex models and two-dimensional turbulence, *Phys. Fluids*, *7*, 2465–2474, 1994.

Bell, G. D., and L. F. Bosart, A 15-year climatology of Northern hemisphere 500 mb closed cyclone and anticyclone centers, *Mon. Weather Rev.*, *117*, 2142–2163, 1989.

Boville, B. W., The Aleutian stratospheric anticyclone, *J. Meteorol.*, *17*, 329–336, 1960.

Brachet, M. E., M. Meneguzzi, H. Politano, and P. L. Sulem, The dynamics of freely decaying two-dimensional turbulence, *J. Fluid Mech.*, *194*, 333–349, 1988.

Butchart, N., and E. E. Remsberg, The area of the stratospheric polar vortex as a diagnostic for tracer transport on an isentropic surface, *J. Atmos. Sci.*, *43*, 1319–1339, 1986.

Chen, P., J. R. Holton, A. O'Neill, and R. Swinbank, Isentropic mass exchange between the Tropics and extratropics in the stratosphere, *J. Atmos. Sci.*, *51*, 3006–3018, 1994.

Dameris, M., and V. Grewe, Three-dimensional description of the stratospheric polar vortex, *Beitr. Phys. Atmos.*, *67*, 157–160, 1994.

Dameris, M., M. Wirth, W. Renger, and V. Grewe, Definition of the polar vortex edge by LIDAR data of the stratospheric aerosol: A comparison with values of potential vorticity, *Beitr. Phys. Atmos.*, *68*(2), 113–119, 1995.

Degorska, M., and B. Rajewska-Wiech, The role of stratospheric minor warmings in producing the total ozone deficiencies over Europe in 1992 and 1993, *J. Atmos. Terr. Phys.*, *58*, 1855–1862, 1996.

Dewar, W. K., and G. R. Flierl, Particle trajectories and simple models of transport in coherent vortices, in *Dynamics of Atmospheres and Oceans*, pp. 215–252, Elsevier Sci., New York, 1985.

Domon, K., I. Osamu, and S. Watanabe, Mass transport by a vortex ring, *J. Phys. Soc. Jpn.*, *69*, 120–123, 2000.

Elhmaidi, D., A. Provenzale, and A. Babiano, Elementary topology of two dimensional turbulence from a Lagrangian viewpoint and single particle dispersion, *J. Fluid Mech.*, *257*, 533–558, 1993.

Fairlie, T. D. A., Three-dimensional transport simulations of the dispersal of volcanic aerosol from Mount Pinatubo, *Q. J. R. Meteorol. Soc.*, *121*, 1943–1980, 1995.

Fairlie, T. D. A., and A. O'Neill, The stratospheric major warming of winter 1984/85: Observations and dynamical inferences, *Q. J. R. Meteorol. Soc.*, *114*, 557–577, 1988.

Fairlie, T. D. A., A. O'Neill, and V. D. Pope, The sudden breakdown of an unusually strong cyclone in the stratosphere during winter 1988/89, *Q. J. R. Meteorol. Soc.*, *116*, 767–774, 1990.

Fairlie, T. D. A., R. B. Pierce, J. A. Al-Saadi, W. L. Grose, J. M. Russell III, M. H. Proffitt, and C. R. Webster, The contribution of mixing in Lagrangian photochemical predictions of polar ozone loss over the Arctic in summer 1997, *J. Geophys. Res.*, *104*, 26,597–26,609, 1999.

Farrara, J. D., M. Fisher, and C. R. Mechoso, Planetary-scale disturbances in the southern stratosphere during early winter, *J. Atmos. Sci.*, *49*, 1757–1775, 1992.

Hartmann, D., et al., Transport into the South Polar vortex in early spring, *J. Geophys. Res.*, *94*, 16,779–16,796, 1989.

Harvey, V. L., and M. H. Hitchman, A climatology of the Aleutian High, *J. Atmos. Sci.*, *53*, 2088–2101, 1996.

Haynes, P. H., High-resolution three-dimensional modelling of stratospheric flows: Quasi-two dimensional turbulence dominated by a single vortex, in *Topological Fluid Mechanics*, edited by H. K. Moffat and A. Tsinober, Cambridge Univ. Press, New York, 1990.

Hirota, I., K. Saotome, T. Suzuki, and S. Ikeda, Structure and behavior of the Aleutian anticyclone as revealed by meteorological rocket and satellite observations, *J. Meteorol. Soc. Jpn.*, *51*, 353–362, 1973.

Hitchman, M. H., et al., Mean winds in the tropical stratosphere and mesosphere during January 1993, March 1994, and August 1994, *J. Geophys. Res.*, *102*, 26,033–26,052, 1997.

Hsu, C.-P., Air parcel motions during a numerically simulated sudden stratospheric warming, *J. Atmos. Sci.*, *37*, 2768–2792, 1980.

Jones, D. A., and I. Simmonds, A climatology of Southern hemisphere extratropical cyclones, *Clim. Dyn.*, *9*, 131–145, 1993.

Jones, D. A., and I. Simmonds, A climatology of Southern hemisphere anticyclones, *Clim. Dyn.*, *10*, 333–348, 1994.

Knox, J. A., Generalized nonlinear balance criteria and inertial stability, *J. Atmos. Sci.*, *54*, 967–985, 1997.

Koh, T.-Y., and R. A. Plumb, Lobe dynamics applied to barotropic Rossby-wave breaking, *Phys. Fluids*, *12*, 1518–1528, 2000.

Labitzke, K., Interannual variability of the winter stratosphere in the northern hemisphere, *Mon. Weather Rev.*, *105*, 762–770, 1977.

Labitzke, K., Stratospheric-mesospheric midwinter disturbances: A summary of observed characteristics, *J. Geophys. Res.*, *86*, 9665–9678, 1981a.

Labitzke, K., The amplification of height-wave 1 in January 1979: A characteristic precondition for the major warming in February, *Mon. Weather Rev.*, *109*, 983–989, 1981b.

Lahoz, W. A., et al., Vortex dynamics and the evolution of water vapour in the stratosphere of the southern hemisphere, *Q. J. R. Meteorol. Soc.*, *122*, 423–450, 1996.

Lambert, S. J., A cyclone climatology of the Canadian Climate Centre general circulation model, *J. Clim.*, *1*, 109–115, 1988.

Malvern, L. E., *Introduction to the Mechanics of a Continuous Medium*, Prentice-Hall, Old Tappan, N. J., 713 pp., 1969.

Manney, G. L., and R. W. Zurek, Interhemispheric comparison of the development of the stratospheric polar vortex during fall: A 3-dimensional perspective for 1991–1992, *Geophys. Res. Lett.*, *20*, 1275–1278, 1993.

Manney, G. L., R. W. Zurek, M. E. Gelman, A. J. Miller, and R. Nagatani, The anomalous Arctic lower stratospheric polar vortex of 1992–1993, *Geophys. Res. Lett.*, *21*, 2405–2408, 1994.

Manney, G. L., et al., Formation of low-ozone pockets in the middle stratospheric anticyclone during winter, *J. Geophys. Res.*, *100*, 13,939–13,950, 1995a.

Manney, G. L., et al., Lagrangian transport calculations using UARS data, part I, Passive tracers, *J. Atmos. Sci.*, *52*, 3049–3068, 1995b.

Manney, G. L., W. A. Lahoz, and R. W. Zurek, Simulation of the December 1998 stratospheric major warming, *Geophys. Res. Lett.*, *26*, 2733–2736, 1999.

Manney, G. L., H. A. Michelsen, F. W. Irion, G. C. Toon, M. R. Gunson, and A. E. Roche, Lamination and polar vortex development in fall from ATMOS long-lived trace gases observed during November 1994, *J. Geophys. Res.*, *105*, 29,023–29,038, 2000.

McIntyre, M. E., How well do we understand the dynamics of stratospheric warmings?, *J. Meteorol. Soc. Jpn.*, *60*, 37–65, 1982.

McIntyre, M. E., and T. N. Palmer, Breaking planetary waves in the stratosphere, *Nature*, *305*, 593–600, 1983.

McIntyre, M. E., and T. N. Palmer, The "surf zone" in the stratosphere, *J. Atmos. Terr. Phys.*, *46*, 825–849, 1984.

McWilliams, J. C., The emergence of isolated coherent vortices in turbulent flow, *J. Fluid Mech.*, *146*, 21–34, 1984.

Mechoso, C. R., and D. L. Hartmann, An observational study of traveling planetary waves in the southern hemisphere, *J. Atmos. Sci.*, *39*, 1921–1935, 1982.

Mechoso, C. R., A. O'Neill, V. D. Pope, and J. D. Farrara, A study of the stratospheric final warming of 1982 in the southern hemisphere, *Q. J. R. Meteorol. Soc.*, *49*, 1242–1263, 1988.

Mechoso, C. R., J. D. Farrara, and M. Ghil, Intraseasonal variability of the winter circulation in the southern hemisphere atmosphere, *J. Atmos. Sci.*, *48*, 1387–1404, 1991.

Michelsen, H. A., G. L. Manney, M. R. Gunson, C. P. Rinsland, and R. Zander, Correlations of stratospheric abundances of CH_4 and N_2O derived from ATMOS measurements, *Geophys. Res. Lett.*, *25*, 2777–2780, 1998.

Michelsen, H. A., et al., Intercomparison of ATMOS, SAGE II and ER-2 observations in Arctic vortex and extra-vortex air masses during spring 1993, *Geophys. Res. Lett.*, *26*, 291–294, 1999.

Morris, G. A., S. R. Kawa, A. R. Douglass, M. R. Schoeberl, L. Froidevaux, and J. Waters, Low-ozone pockets explained, *J. Geophys. Res.*, *103*, 3599–3610, 1998.

Murray, R. J., and I. Simmonds, A numerical scheme for tracking cyclone centres from digital data, part I, development and operation of the scheme, *Aust. Meteorol. Mag.*, *39*, 155–166, 1991.

Nash, E. R., P. A. Newman, J. E. Rosenfield, and M. R. Schoeberl, An objective determination of the polar vortex using Ertel's potential vorticity, *J. Geophys. Res.*, *101*, 9471–9478, 1996.

Norton, W. A., and G. D. Carver, Visualizing the evolution of the stratospheric polar vortex in January 1992, *Geophys. Res. Lett.*, *21*, 1455–1458, 1994.

O'Neill, A., and V. D. Pope, Simulations of linear and nonlinear disturbances in the stratosphere, *Q. J. R. Meteorol. Soc.*, *114*, 1063–1110, 1988.

O'Neill, A., W. Grose, V. D. Pope, H. Maclean, and R. Swinbank, Evolution of the stratosphere during Northern winter 1991/92 as diagnosed from U. K. Meteorological Office analyses, *J. Atmos. Sci.*, *51*, 2800–2817, 1994.

Paparella, F., A. Babiano, C. Basdevant, A. Provenzale, and P. Tanga, A Lagrangian study of the Antarctic polar vortex, *J. Geophys. Res.*, *102*, 6765–6773, 1997.

Pawson, S., K. Labitzke, R. Lenschow, B. Naujokat, B. Rajewski, M. Wiesner, and R.-C. Wohlfart, Climatology of the Northern Hemisphere stratosphere derived from Berlin analyses, part 1, Monthly means, in *Meteorologische Abhandlungen*, vol. 7, no. 3, Von Dietrich Reimer, Berlin, 1993.

Pierce, R. B., and T. D. A. Fairlie, Chaotic advection in the stratosphere: Implications for the dispersal of chemically perturbed air from the polar vortex, *J. Geophys. Res.*, *98*, 18,589–18,595, 1993.

Pierce, R. B., W. T. Blackshear, T. D. Fairlie, W. L. Grose, and R. E. Turner, The interaction of radiative and dynamical processes during a simulated sudden stratospheric warming, *J. Atmos. Sci.*, *50*, 3829–3851, 1993.

Polvani, L. M., and R. Saravanan, The three-dimensional structure of breaking Rossby waves in the polar wintertime stratosphere, *J. Atmos. Sci.*, *57*, 3663–3685, 2000.

Polvani, L. M., D. W. Waugh, and R. A. Plumb, On the subtropical edge of the stratospheric surf zone, *J. Atmos. Sci.*, *52*, 1288–1309, 1995.

Price, J. D., and G. Vaughan, Statistical studies of cut-off-low systems, *Ann. Geophys.*, *10*, 96–102, 1992.

Provenzale, A., Transport by coherent barotropic vortices, *Annu. Rev. Fluid Mech.*, *31*, 55–93, 1999.

Randel, W. J., and F. Wu, Cooling of the Arctic and Antarctic polar stratospheres due to ozone depletion, *J. Clim.*, *12*, 1467–1479, 1999.

Randel, W. J., et al., Stratospheric transport from the tropics to middle latitudes by planetary-wave mixing, *Nature*, *365*, 533–535, 1993.

Rosier, S. M., and B. N. Lawrence, The January 1992 stratospheric sudden warming: A role for tropical inertial instability?, *Q. J. R. Meteorol. Soc.*, *125*, 2575–2596, 1999.

Rummukainen, M., B. Knudsen, and P. von der Gathen, Dynamical diagnostics of the edges of the polar vortices, *Ann. Geophys.*, *12*, 1114–1118, 1994.

Salby, M. L., D. O'Sullivan, R. R. Garcia, and P. Callaghan, Air motions accompanying the development of a planetary wave critical layer, *J. Atmos. Sci.*, *47*, 1179–1204, 1990.

Scherhag, R., Die explosionsartigen Stratospharenerwarmungen des Spatwinters 1952, *Ber. Dtsch. Wetterdienstes (US Zone)*, *38*, 51–63, 1952.

Schoeberl, M. R., L. R. Lait, P. A. Newman, and J. E. Rosenfield, The structure of the polar vortex, *J. Geophys. Res.*, *97*, 7859–7882, 1992.

Shiotani, M., K. Kuroi, and I. Hirota, Eastward traveling waves in the southern hemisphere stratosphere during the spring of 1983, *Q. J. R. Meteorol. Soc.*, *116*, 913–927, 1990.

Simmonds, I., and X. Wu, Cyclone behaviour response to changes in winter southern hemisphere sea-ice concentration, *Q. J. R. Meteorol. Soc.*, *119*, 1121–1148, 1993.

Sinclair, M. R., An objective cyclone climatology for the Southern hemisphere, *Mon. Weather Rev.*, *122*, 2239–2256, 1994.

Sinclair, M. R., A climatology of cyclogenesis for the Southern hemisphere, *Mon. Weather Rev.*, *123*, 1602–1619, 1995.

Sinclair, M. R., A climatology of anticyclones and blocking for the Southern hemisphere, *Mon. Weather Rev.*, *124*, 245–263, 1996.

Sinclair, M. R., Objective identification of cyclones and their circulation intensity, and climatology, *Weather Forecast.*, *12*, 595–612, 1997.

Swinbank, R., and A. O'Neill, A stratosphere-troposphere data assimilation system, *Mon. Weather Rev.*, *122*, 686–702, 1994.

Thorncroft, C. D., B. J. Hoskins, and M. E. McIntyre, Two paradigms of baroclinic-wave life-cycle behaviour, *Q. J. R. Meteorol. Soc.*, *119*, 17–55, 1993.

Trounday, B., L. Perthuis, S. Strebelle, J. D. Farrara, and C. R. Mechoso, Dispersion properties of the flow in the southern stratosphere during winter and spring, *J. Geophys. Res.*, *100*, 13,901–13,918, 1995.

Wang, K.-Y., and D. E. Shallcross, A Lagrangian study of the three-dimensional transport of boundary-layer tracers in an idealised baroclinic wave live-cycle, *J. Atmos. Chem.*, *35*, 227–247, 2000.

Warn, T., and H. Warn, The evolution of a nonlinear critical level, *Stud. Appl. Math.*, *59*, 37–71, 1978.

Waugh, D. W., Subtropical stratospheric mixing linked to disturbances in the polar vortices, *Nature*, *365*, 535–537, 1993.

Waugh, D. W., Elliptical diagnostics of stratospheric polar vortices, *Q. J. R. Meteorol. Soc.*, *123*, 1725–1748, 1997.

Waugh, D. W., and D. G. Dritschel, The Dependence of Rossby Wave Breaking on the Vertical Structure of the Polar Vortex, *J. Atmos. Sci.*, *56*, 2359–2375, 1999.

Waugh, D. W., and W. J. Randel, Climatology of Arctic and Antarctic polar vortices using elliptical diagnostics, *J. Atmos. Sci.*, *56*, 1594–1613, 1999.

Waugh, D. W., et al., Fine-scale, poleward transport of tropical air during AASE 2, *Geophys. Res. Lett.*, *21*, 2603–2606, 1994.

Waugh, D. W., W. J. Randel, S. Pawson, P. A. Newman, and E. R. Nash, Persistence of the lower stratospheric polar vortices, *J. Geophys. Res.*, *104*, 27,191–27,201, 1999.

Weiss, J. B., Transport and mixing in traveling waves, *Phys. Fluids A*, *5*, 1379–1384, 1991a.

Weiss, J. B., The dynamics of entropy transfer in two-dimensional hydrodynamics, *Physica*, 273–294, 1991b.

Yang, H., Three-dimensional transport of the Ertel potential vorticity and N_2O in the GFDL SKYHI Model, *J. Atmos. Sci.*, *52*, 1513–1528, 1995.

Yoden, S., T. Yamaga, S. Pawson, and U. Langematz, A composite analysis of the stratospheric sudden warmings simulated in a perpetual January integration of the Berlin TSM GCM, *J. Meteorol. Soc. Jpn.*, *77*, 431–445, 1999.

Zhou, S., M. E. Gelman, and A. J. Miller, An inter-hemisphere comparison of the persistent stratospheric polar vortex, *Geophys. Res. Lett.*, *27*, 1123–1126, 2000.

T. D. Fairlie and R. B. Pierce, NASA Langley Research Center, Hampton, VA, USA.

V. L. Harvey, Science Applications International Corporation, MS 401B, Hampton, VA 23681, USA. (v.l.harvey@larc.nasa.gov)

M. H. Hitchman, Department of Atmospheric and Oceanic Sciences, University of Wisconsin - Madison, Madison, WI, USA.

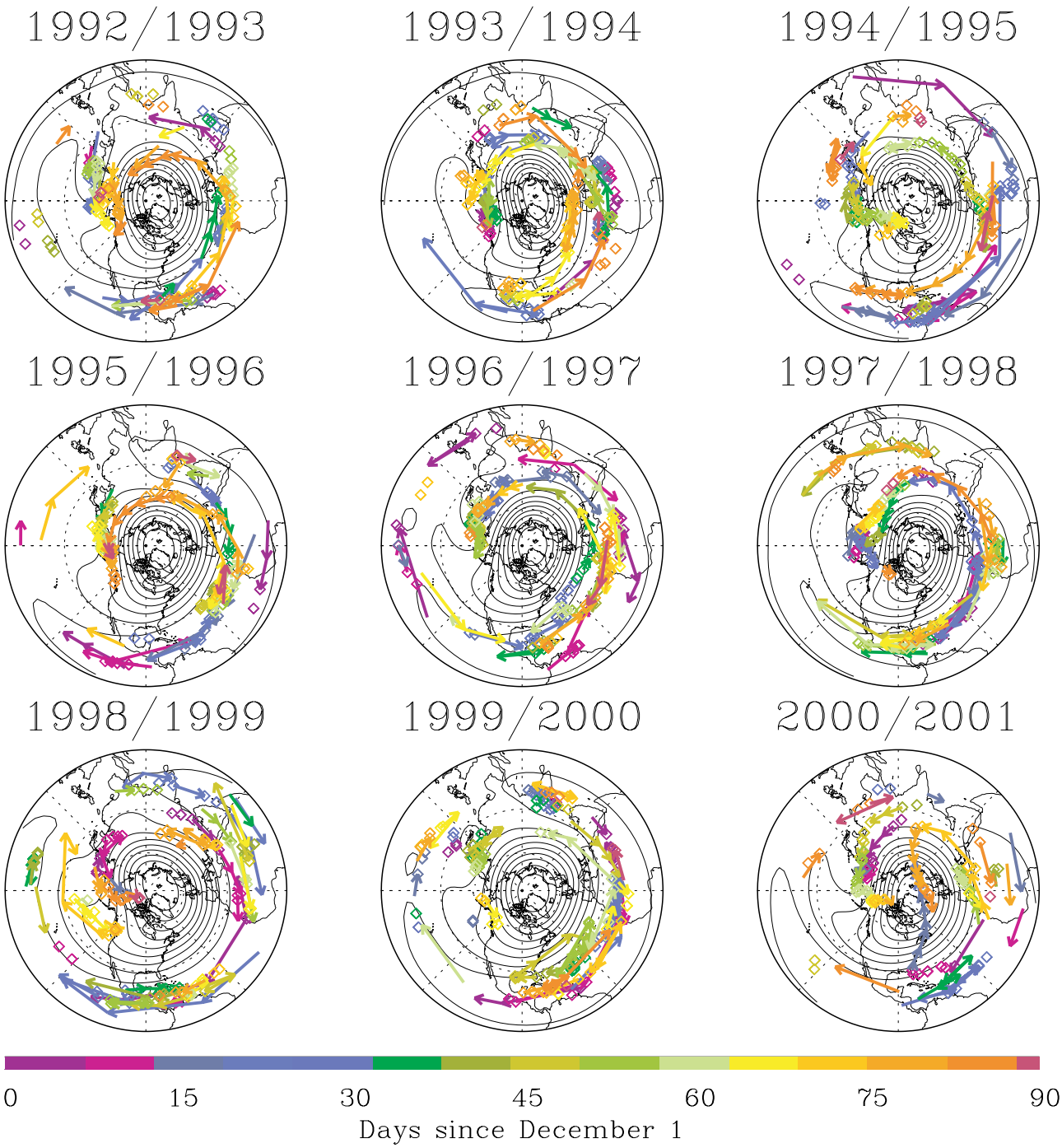

Figure 13. Daily position and movement of Northern Hemisphere anticyclones for each DJF season from 1992 to 2001 on the 1200 K isentropic surface. Contour interval is 10%.

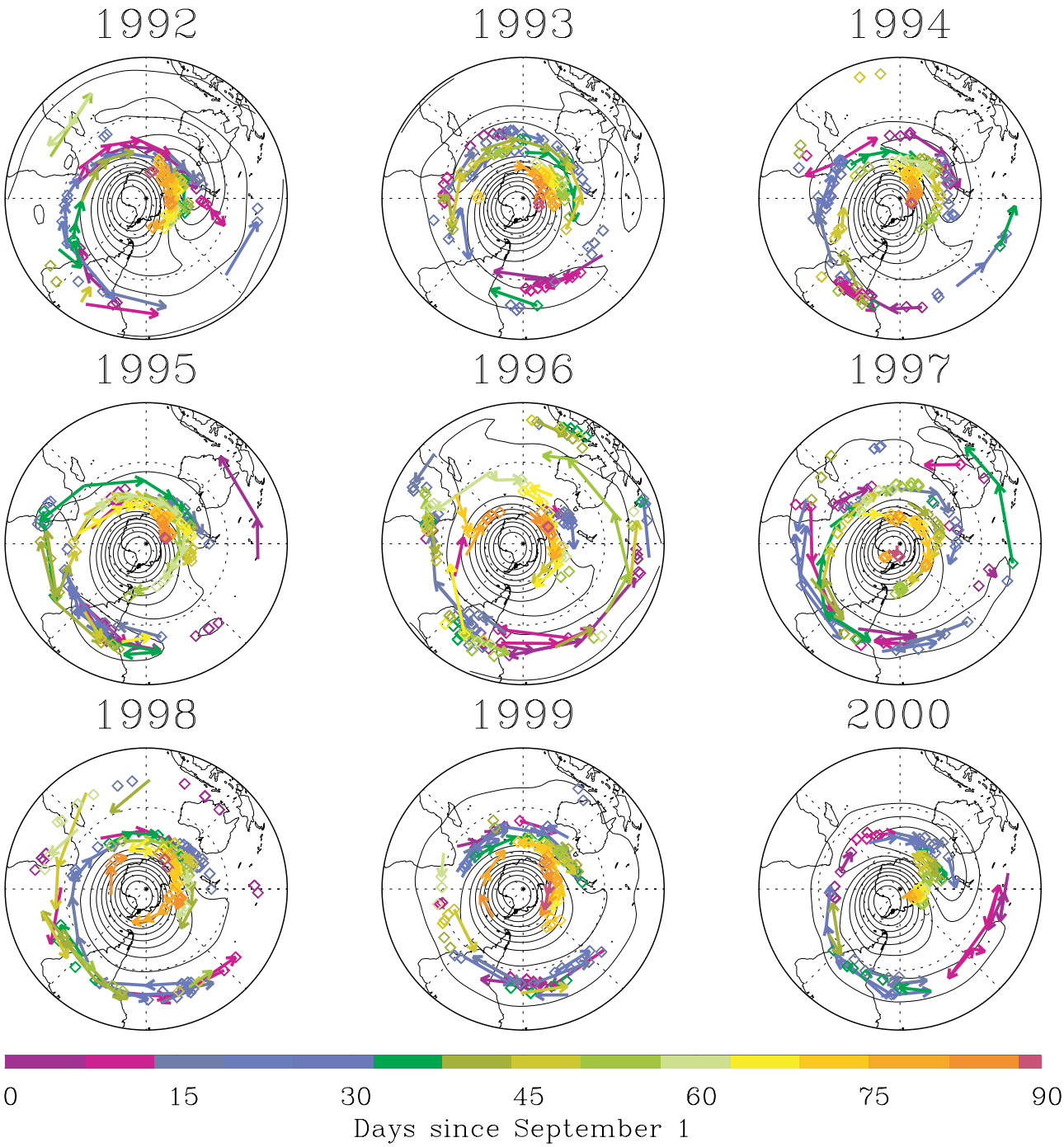

Figure 14. As Figure 13 in the Southern Hemisphere during SON.